



HAWC+

Handbook for Archive Users

Peter Ashton
Sarah Eftekharzadeh
Sachindev S. Shenoy

Rev 1.0
Date: 2023 Sep 27

HAWC+ Handbook for Archive Users

Table of Contents

1. ESSENTIAL INFORMATION	1
2. INSTRUMENT DESCRIPTION	3
2.1 HAWC+ OVERVIEW	3
2.2 OBSERVATIONAL CONFIGURATION AND MODES	5
2.2.1 <i>Nod-Match-Chop Mode</i>	5
2.3 ON-THE-FLY MAPPING (OTFMAP)	7
2.3.1 <i>History of OTFMAP Polarimetry</i>	8
2.3.2 <i>HAWC+ Band B Warning</i>	8
3. INSTRUMENT PERFORMANCE.....	9
3.1 OVERVIEW	9
3.2 SENSITIVITY	9
3.3 DATA QUALITY CHARACTERISTICS OVER TIME	10
3.3.1 <i>Full Width Half Maximum</i>	10
3.3.2 <i>Flux Calibration Variability</i>	11
4. DATA	14
4.1 DATA PRODUCT & FORMAT	14
4.1.1 <i>File Naming Conventions</i>	14
4.1.2 <i>Data Format</i>	14
4.1.3 <i>Pipeline Products</i>	14
4.2 CORRECTION FOR ATMOSPHERIC OPACITY	16
4.3 FLUX CALIBRATION	17
4.3.1 <i>Instrumental Polarization</i>	18
4.3.2 <i>Internal Calibrator</i>	18
4.4 DATA ARTIFACT	18
4.5 KNOWN ARTIFACTS & MITIGATION	21
4.5.1 <i>Dark outline around an extended emission</i>	21
4.5.2 <i>Low Scan Velocity Bleed Through</i>	21
4.5.3 <i>Low CentroidExpMsec</i>	23
4.5.4 <i>Tracking Error I</i>	26
4.5.5 <i>Tracking Error II</i>	26
4.5.6 <i>Incomplete HWP</i>	28
4.5.7 <i>URD Vignetting</i>	29
4.5.8 <i>Double Source</i>	30
4.5.9 <i>“Peanut” PSF</i>	32
4.6 AN EXAMPLE OF BASIC POLARIZATION DATA INSPECTION AND VISUALIZATION	33
4.7 OBSERVATIONS AT HIGHER TEMPERATURE	33
5. SCIENTIFIC RESULTS	35
5.1 EXTENDED SOURCE POLARIMETRY	35
5.2 HAWC LEGACY SURVEYS	35
5.2.1 <i>FIELDMAPS: Filaments Extremely Long and Dark: A Magnetic Polarization Survey</i>	35
5.2.2 <i>SALSA: SOFIA Heralds a New Era of Measuring the Magnetic Fields of Galaxies</i>	36
5.2.3 <i>A Two-Color Polarimetric Survey of the Galactic Center</i>	37
5.2.4 <i>Study of Interstellar Magnetic Polarization: A Legacy Investigation of Filaments (SIMPLIFI)</i>	37

6. REFERENCES	39
APPENDIX	40
A. RESPONSE/TRANSMISSION CURVES	40
B. HISTORICAL FWHM AND CALIBRATION FACTORS	41
C. COLOR CORRECTION FACTORS	44
D. IMPORTANT HAWC+ HEADER KEYWORDS.....	46
D.1 HISTORY Section of HAWC+ FITS Data Headers	50

1. ESSENTIAL INFORMATION

Table 1: HAWC+ Instrument Characteristics

Parameters	Units	Band A	Band B	Band C	Band D	Band E
Mean Wavelength (λ_0)	μm	53	63	89	154	214
Band Width ($\Delta\lambda$) ¹	-	8.70	8.90	17.00	34.00	44.00
Filter Width ($\Delta\lambda/\lambda$)	-	0.171	0.150	0.194	0.219	0.204
Beam Size (FWHM)	arcsec	4.85	10.50	7.80	13.60	18.20
Pixel Size ²	arcsec	2.55	4.00	4.02	6.90	9.37
Total Intensity FOV	arcmin	2.8×1.7	4.2×2.7	4.2×2.7	7.4×4.6	8.4×6.2
Polarimetry FOV	arcmin	1.4×1.7	2.1×2.7	2.1×2.7	3.7×4.6	4.2×6.2
NESB ³ (photo)	MJy sr ⁻¹ h ^{1/2}	18.8	11.4	6.3	1.6	0.8
MDCF ⁴	mJy	250	400	300	260	230
Mapping Speed ⁵	⁵	0.0027	0.0290	0.0290	1.1000	7.0000
MDCPF ⁶	Jy	80	150	50	50	50
IP ⁷	q	-0.0154	-	-0.0151	0.0028	-0.0129
	u	-0.0030	-	0.0090	0.0191	0.0111
MIFP	MJy sr ⁻¹ h ^{1/2}	28,000	17,000	6,000	2,000	1,300

¹ See the filter response curves in [Figure 28](#).

² The center-to-center spacing of the pixels; pixel sizes (the space taken up by the photon sensitive area) are smaller by 0.21 arcsec at 53 μm and 0.75 arcsec at 215 μm .

³ Noise Equivalent Surface Brightness for S/N = 1 into a single HAWC+ beam (FWHM given here).

⁴ Minimum Detectable Continuum Flux for a point source with S/N = 4 in a 900 second integration.

⁵ Real scan rate required to achieve a given NESB. Units: arcmin² h⁻¹ (MJy sr⁻¹)².

⁶ Minimum Total Continuum Flux for a point source required to measure the polarization fraction to an uncertainty level of $\sigma_p < 0.3\%$ with a SNR (in the polarization fraction) ≥ 4 in 900s.

⁷ Instrumental Polarization estimated using the observations of planets during several observing runs. The uncertainty of the instrumental polarization is smaller than 0.003 in both Stokes q and u. IP for Band B is still TBD.

Table 2: HAWC+ Flight Series Information

Flight Series	Flight Numbers	Deploy Location	Start Date	End Date
Commissioning I	F293 – F295	Palmdale, CA	04/28/2016	05/05/2016
Commissioning II	F334 – F335	Palmdale, CA	09/30/2016	10/07/2016
OC4L	F353 – F360	Palmdale, CA	11/28/2016	12/16/2016
OC5E	F393 – F397	Palmdale, CA	05/02/2017	05/16/2017
OC5N	F440 – F454	Palmdale, CA	10/11/2017	11/17/2017
OC6I	F480 – F487	Christchurch, NZ	08/20/2018	09/14/2018
OC6K	F504 – F513	Palmdale, CA	09/15/2018	10/12/2018
OC6T	F545 – F547	Palmdale, CA	02/08/2019	02/21/2019
OC7E	F596 – F601	Christchurch, NZ	07/13/2019	08/06/2019
OC7F	F605 – F621	Palmdale, CA ¹	08/30/2019	10/04/2019
OC7J	F650 – F657	Palmdale, CA	01/11/2021	01/31/2021
OC8E	F683 – F690	Palmdale, CA	09/08/2020	09/25/2020
OC8K	F726 – F736	Palmdale, CA	04/15/2021	05/21/2021

OC9D	F774 – F784	Palmdale, CA	08/21/2021	09/13/2021
OC9E	F786 – F788	Palmdale, CA	10/23/2021	11/12/2021
OC9H	F800 – F802	Palmdale, CA	12/05/2021	12/23/2021
OC9Q	F879 – F886	Palmdale, CA	05/28/2022	06/10/2022
OC9R	F889 – F895	Christchurch, NZ	06/20/2022	07/07/2021
OC9W	F916 – F921	Palmdale, CA	09/20/2022	09/29/2022

¹Flight F611 on 09/18/2019 was deployed out of Stuttgart, Germany.

Important HAWC+ resources:

- [Pipeline tutorial document](#)
- [Pipeline tutorial video from pipeline week](#)
- [Calibration video from SOFIA School](#)
- [Data Reduction Pipeline User's Manual](#)
- [Principal Reference Paper on HAWC+](#)

2. INSTRUMENT DESCRIPTION

2.1 HAWC+ OVERVIEW

The High-resolution Airborne Wideband Camera (HAWC+) was a multi-wavelength far-infrared imager and polarimeter with continuum band passes from 50 μm to 240 μm . HAWC+ Total Intensity Imaging used a filter wheel and a polarizing grid to split incoming light into two orthogonal components of lineal polarization, the reflected (R) and transmitted (T) rays. For Imaging Polarimetry, a rotating half-wave plate (HWP) was introduced before the filter wheels. The instrument included a 64x40 array measuring the R polarization state and a 32x40 array for the T polarization state. HAWC+ observations were diffraction-limited with a spatial resolution of 5 to 20 arcsec and a field of view (FOV) of ~ 2 to 10 arcmin. The following section provides a brief introduction to the HAWC+ instrument, observing configuration and its operating modes. For a more complete description, see the instrument paper by ([Harper et al. 2018](#), hereafter [H18](#)).

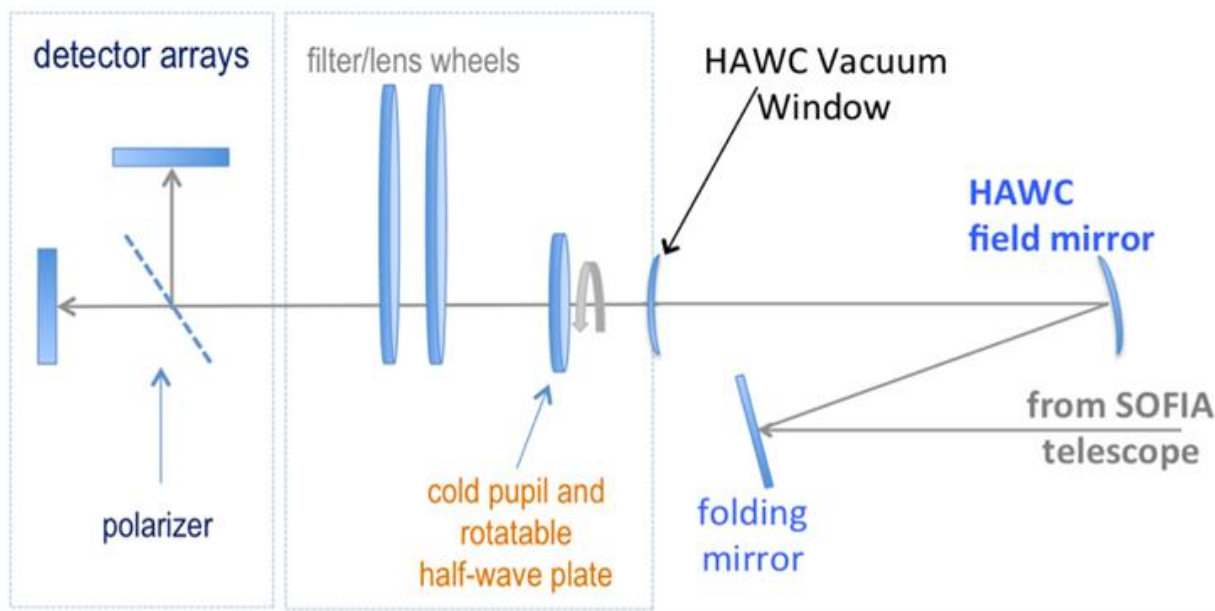


Figure 1 *Fore optics components and the light path.*

A schematic of the HAWC+ optical design is shown in [Figure 1](#). Prior to entering the HAWC+ cryostat, light from the SOFIA telescope entered the set of warm fore-optics. The light was reflected from a folding mirror to a field mirror, capable of imaging the SOFIA pupil at the cold pupil inside the HAWC+ cryostat. After the fore-optics, light entered the cryostat through a 7.6 cm diameter high-density polyethylene (HDPE) window, it passed through a cold pupil on a rotatable carousel, near-infrared blocking filters to define each bandpass, and lenses designed to optimize the plate scale. The pupil carousel and the filter wheel were at a temperature of ~ 10 K. The carousel contained eight aperture positions, four of which contained half wave plates (HWPs) for HAWC+ bands, an open aperture whose diameter was matched to the SOFIA pupil, and three aperture options meant only for instrument alignment tests.

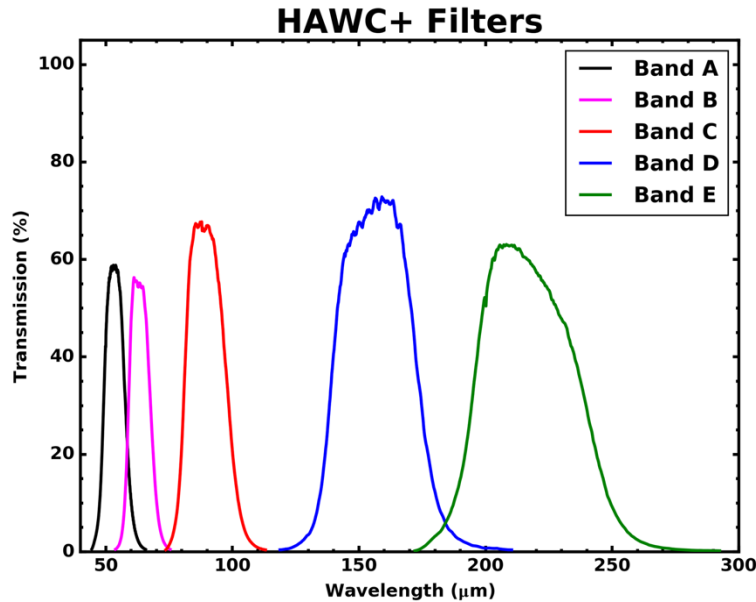


Figure 2 *HAWC+ Filter Transmission*

The light then passed through the filter wheel, where five filters were available, labeled ‘A’ through ‘E’ in ascending order of wavelength. See [Figure 2](#) and [Table 1](#) for filter characteristics.

After the filter carousel, the light passed through a wire grid, which was heat-sunk to the HAWC+ 1 Kelvin stage, that reflected one component of linear polarization and transmitted the orthogonal component to the detector arrays (R and T arrays, respectively—see [Figure 3](#)). The R array was populated with two 32x40 subarrays separated by 2.0 pixels, referred to as R0 (top left) and R1 (top right). The arrays were coaligned such that R0 and T0 (bottom left) observed the same patch of sky. Polarization observations were *only* supported using the R0 and T0 subarrays, and therefore observations were limited to the left half of the nominal field of view, or 32x40 pixels. Total intensity observations were supported using the combined R0 and R1 field of view, or 64x40 pixels with a 2.0-pixel gap between them.

To perform polarimetry observations, an HWP matched to the band-pass was rotated (usually through four discrete angles) to modulate the incident light and allow computation of the Stokes parameters. The total intensity could be measured simply by removing the HWPs from the optical path and using the open pupil position, then summing the signal from the R and T arrays.

The 64x40 HAWC+ detector array was composed of two co-mounted 32x40 subarrays from NASA/GSFC and National Institute of Standards and Technology (NIST). The detectors were superconducting transition-edge sensor (TES) thermometers on membranes with a wide-band absorber coating. The detector array was an indium bump bonded to a matched array of superconducting quantum interference device (SQUID) amplifiers, all cooled to an operating temperature of ~0.2 K in flight.

[Figure 3](#) shows HAWC+ TES detector subarrays. R0 and R1 detected the reflected component of linear polarization and T0 detected the orthogonal component, the transmitted polarization.

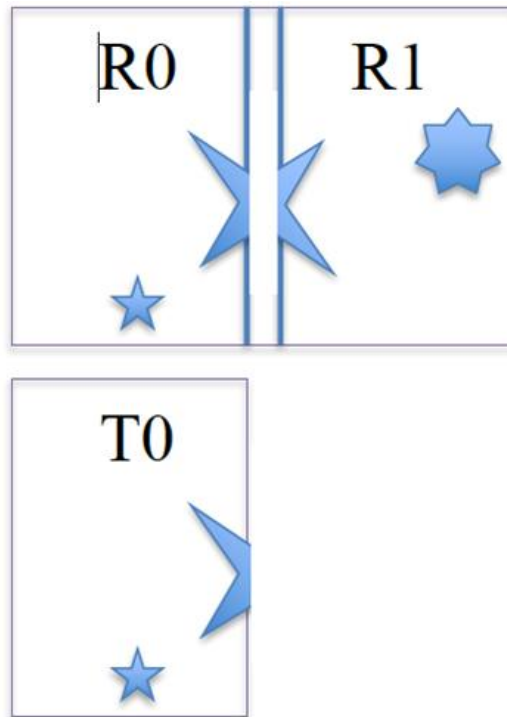


Figure 3 *HAWC+ TES detector subarrays.*

2.2 OBSERVATIONAL CONFIGURATION AND MODES

The HAWC+ instrument had two instrument configurations for imaging (commonly referred to as Total Intensity) and polarization observations. In both types of observations, removing background flux due to the telescope and sky was a challenge that required one of several observational strategies. The HAWC+ instrument used the secondary mirror to chop rapidly between two positions (source and sky), used discrete telescope motions to nod between different sky positions, or used slow continuous scans of the telescope across the desired field. In chopping and nodding strategies, sky positions were subtracted from source positions to remove background levels. In scanning strategies, the continuous stream of data was used to solve for the underlying source and background structure.

HAWC+ had two standard observing modes for imaging: the Nod-Match-Chop (NMC) instrument mode which combined traditional chopping with nodding and the On-The-Fly Mapping (OTFMAP) mode which used slow telescope scans without chopping. Likewise, polarization observations could be taken in either Nod-Pol or Scan-Pol mode. Nod-Pol mode included chopping and nodding cycles in multiple HWP positions; Scan-Pol mode included repeated scans at multiple HWP positions.

2.2.1 Nod-Match-Chop Mode

To remove the background from the mid-infrared (MIR) image and detect the faint astronomical sources, observations of another region (free of sources) were made, and the two images were

subtracted. However, since the MIR is highly variable, both spatially and temporally, it would take far too long (on the order of seconds) to reposition a large telescope to observe this sky background region. By the time the telescope had moved and settled at the new location; the sky background level would have changed so much that the subtraction of the two images would be useless. To avoid this problem, the secondary mirror of the telescope (which was considerably smaller than the primary mirror) was tilted, rather than moving the entire telescope. This allowed observers to look at two different sky positions very quickly (on the order of a few to ten times per second), because tilting the secondary by an angle θ moved the center of the field imaged by the detector by θ on the sky. Tilting the secondary between two positions was known as “chopping”. HAWC+ observations were typically made with a chopping frequency of 10 Hz.

Symmetric Chop:

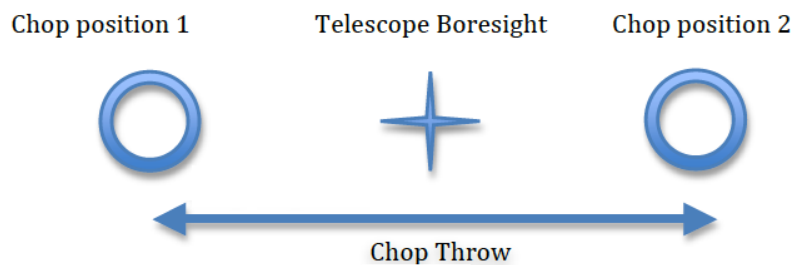


Figure 4 *Symmetric chopping in Nod-Match-Chop (NMC) mode.*

On SOFIA chopping could be done either symmetrically or asymmetrically about the telescope’s optical axis, but HAWC+ used only symmetric chopping where the secondary mirror was tilted symmetrically about the telescope optical axis (also known as the boresight) in the two chop positions. The distance between the two chop positions was known as the chop throw. The distance between the boresight and either chop position was known as the chop amplitude and was equal to half the chop throw as shown in [Figure 4](#).

Unfortunately, moving the secondary mirror caused the telescope to be slightly misaligned, which introduced optical distortions in the images—notably, the optical aberration known as coma and additional background emission from the telescope that was considerably smaller than the sky emission but nonetheless present. The additional telescopic background mentioned could be removed by moving the entire telescope to a new position and then chopping the secondary again between two positions. Subtracting the two chop images at this new telescope position would remove the sky emission but leave the additional telescopic background due to the misalignment; subtracting the result from the chop-subtracted image at the first telescope position would then remove the background.

Since the process of moving to a new position was needed to remove the additional background from the telescope, not the sky, it could be done on a much longer timescale. (The variation in the telescopic backgrounds occurred on timescales on the order of tens of seconds to minutes, much slower than that of the variation in the sky emission.) This movement of the entire telescope, on a much longer timescale than chopping, was known as “nodding”. The two nod positions were usually referred to as nod A and nod B. The distance between the two nod positions was known as the nod throw.

The chop-subtracted images at nod Position B were then subtracted from the chop-subtracted images at nod position A. The result would be an image of the region, without the sky background emission or the additional emission resulting from tilting the secondary during the chopping process. The sequence of chopping in one telescope position, nodding, and chopping again in a second position was known as a chop-nod cycle.

Again, because the Infrared (IR) sky is so bright, deep images of a region could not be obtained (as they are in the optical) by simply observing the region for a long time with the detector collecting photons (integrating) continuously. As stated above, the observations required chopping and nodding at frequent intervals. Hence deep observations were made by effectively stacking a series of chop/nod images. Furthermore, IR detectors are not perfect, and often have bad pixels or flaws. To avoid these defects on the arrays, and prevent them from marring the final images, observers employed a technique known as dithering. Dithering entailed moving the position of the telescope slightly with respect to the center of the region observed each time a new chop/nod cycle was begun, or after several chop/nod cycles. When the images were processed, the observed region would appear in a slightly different place on the detector. This means that the bad pixels did not appear in the same place relative to the observed region. The individual images could then be registered and averaged or median-ed, a process that would eliminate (in theory) the bad pixels from the final image.

2.3 ON-THE-FLY MAPPING (OTFMAP)

In OTFMAP mode, the secondary mirror remained stationary on the optical axis of the telescope while the telescope assembly itself slowly moved with respect to the sky. This scan motion modulated the celestial source with respect to the atmosphere in a manner similar to chopping the secondary mirror. Scan rates had to reach (~ 2 Hz) \times (HAWC+ beam width) to remove the source from the atmospheric background. This implies rates ~ 10 – 80 arcseconds per second depending on the bandpass.

To ensure absolute flux calibration in this mode, observations had to be carefully planned so that the mapped region contained no extended emission from the science target. Otherwise, only a differential flux with respect to the lowest measured intensity level could be measured. Further removal of residual atmospheric signal was performed by removing common-mode noise observed in all HAWC+ detectors. This averaging amounted to a spatial filter with size equal to the HAWC+ FOV. Therefore, while large maps might be necessary to reach a true zero intensity level, not all spatial scales in a given region could be recovered. The OTFMAP in total intensity or polarimetry could be used to map large areas with a potential loss of extended structures larger than 1-2 FOV at a given band.

HAWC+ offered two scan types for OTFMAP scan patterns: Lissajous and Box. Lissajous scans were recommended for sources smaller than the HAWC+ FOV at a given bandpass, while Box scans (analogous to traditional raster scanning methods) were more efficient at mapping large areas several times the FOV. The majority of the HAWC+ OTFMAP data in archive are done using the Lissajous scan pattern, while there are a handful of observations that used Box scans.

2.3.1 History of OTFMAP Polarimetry

As described in [Kovács \(2006\)](#) during this mode, the telescope on its optical axis scanned the intended region by moving on a non-repeating parametric curve at a defined mapping speed. The mapping speed was chosen such that the beam size (FWHM) of the instrument was oversampled at the sampling rate of the detector readout. As in spatial and temporal Nyquist sampling, the sampling rate had to be at least twice the maximum frequency of the astrophysical and/or sky signal and the system noise in this mode had to be kept comparable to or lower than the power spectrum of the sky at the desired spatial frequency to be recovered ([Lopez-Rodriguez et al. 2022](#)) and references therein). Since at any given time, the scan was integrating over a deeper image, this mapping mode reduced the observing overheads as the telescope could be moved to farther adjacent sky regions to reach “true” zero level background emission. For bolometers, the signal was affected by both correlated and uncorrelated 1/f-type noise, from the atmosphere, detectors, and readout electronics, which was characterized by having higher amplitudes at longer timescales. This behavior resulted in signal drifts that could affect all spatial structures in the final image ([Lopez-Rodriguez et al. 2022](#)). Most of the efforts of the OTFMAP strategy focused on the mapmaking algorithms and signal filtering to recover diffuse and extended emission from the astrophysical object. A mapmaking algorithm was required to reconstruct the sky image while subtracting the sky and detector variation responses [Kovács \(2006\)](#). Note that the OTFMAP may also have structures in the background emission that increase with the structure size of the astrophysical object (when the size is larger than the FOV of the array) and inversely with scanning speed.

The OTFMAP observing mode had previously only been used for total intensity observations ([H18](#)). Later observations of galaxies Centaurus A ([Lopez-Rodriguez 2021](#)) and NGC 1097 ([Lopez-Rodriguez et al. 2021](#)) and the molecular clouds Taurus/L1495 ([Li et al. 2022a](#)) and OMC-3/4 ([Li et al. 2022b](#)) reported successfully using the OTFMAP mode with HAWC+ for polarimetric observations. A complete characterization of this new observing mode for HAWC+ is reported in ([Lopez-Rodriguez et al. 2022](#)).

2.3.2 HAWC+ Band B Warning

Historically, Band B has suffered an oversaturation effect that render it unusable, but a cold aperture was installed to minimize the saturation effects. Band B (63 μm) was under commissioning during Cycle 7 but not all the required data could be collected due to flight planning constraint. This band was offered as shared-risk observations during Cycle 8 and 9 and include some data that can be used for characterizing this band. Currently, all the data required for the band characterization can be found in the [IRSA’s SOFIA archive](#).

The data provided in Table 1 for Band B is theoretical and the users should use the existing data from the archive to derive band characteristics before using any of the data for science. There are some science observations for a short list of targets on IRSA, but those observations were coordinated efforts between the instrument team and the investigators of those projects with the objective of further testing and benchmarking the filter characteristics.

3. INSTRUMENT PERFORMANCE

3.1 OVERVIEW

The absorbing coatings on the HAWC+ detector arrays were optimized to produce about 50% efficiency across the wide (50–240 μm) range of bandpasses. The TESs were designed to optimize the sensor time constants and background power at which they saturate, with the goal being operation at both laboratory and stratospheric background levels. The final design included a superconducting transition temperature of ~ 0.3 K and a detector yield of $> 50\%$. Measurements of detector noise showed that their contribution to total measurement uncertainties was negligible such that noise levels were dominated by background photons from the atmosphere.

Measurements of the HAWC+ optical system in the laboratory were consistent with optical models, and flight data have confirmed that the observations were diffraction limited at all wavelengths.

For polarimetry observations, the configuration of HAWC+ lacks a second T polarization state array (as shown in [Figure 3](#)); as such, the field of view is reduced to approximately half in the largest side of the array, providing a 32×40 pixel size rather than 64×40 pixels (the first element of the field of view in [Table 1](#)). Total intensity observations are unaffected and can use the whole field of view via the R polarization state.

Finally, the filter transmission curves (text tables) are available as a zip file the [IRSA SOFIA HAWC+ page](#) and images are shown in the Appendix ([Figure 28](#)) and values related to bandwidth are given in [Table 1](#).

3.2 SENSITIVITY

The sensitivities in [Table 1](#) account for overheads, including nod slew times, bracketing of internal calibrators, and gyro drift checks. On the other hand, the sensitivities provided by the SOFIA Instrument Time Estimator (SITE) only account for on-source time (i.e., integrating time on the source in the FOV of HAWC+); the total overheads of the observations were provided through the Unified SOFIA Proposal and Observation Tool (USPOT) after entering the sensitivity values produced by SITE. Users are requested to use the EXPTIME the fits header keywords, which is the total on-source exposure time, in their data analysis.

HAWC+ point source sensitivities were updated on June 2, 2017, and the values given in [Table 1](#) are based on the in-flight performance of the instrument. Note that values used in previous SOFIA observing cycles (Cycles 4 & 5) were estimates that contained an overestimated point source sensitivity by approximately a factor of two.

Among the designated band passes for HAWC+, band E had the lowest background photon noise ($\sim 2 \times 10^{-16}$ W Hz $^{-1/2}$) which was therefore used as a constraint for the range of desired sensitivity of HAWC+ bolometers. Another sensitivity threshold was determined as the sensitivity that allowed operation without saturation at bands C and D that harbored highest background power per bolometer (~ 60 pW) among the filters (see, e.g., [H18](#) and references therein). The detector arrays

should also be reasonably operable without saturation at room temperatures for lab tests. Note that “saturation” power in TES bolometers refers to the maximum deposited energy in the linear regime which is proportional to heat capacity (not to be confused with saturation concept for CCD pixels). Detector saturation varied between bolometers and across each of the detector subarrays R0, T0, and R1. The design and manufacturing tests concluded that detector yield during nominal operation was dependent on the band pass and the observing condition. [H18](#) reports 72% yield for bands C and D and 74% for band A for bolometers in R0 and T0 subarrays and 50% for bolometers in R1 subarray. The pattern of non-functional detectors due to detector’s electrical problems or multiplexer wiring in each subarray could be seen in the obtained internal calibration (INTCAL) for each filter (see bad pixel mask application in data reduction pipeline manual).

The terminology for quantifying the sensitivity of HAWC+ detectors in imaging and polarimetry modes are Minimum Detectable Continuum Flux (MDCF) and Minimum Detectable Polarized Flux (MDCPF) of a point source and Minimum Intensity for Polarimetry (MIpP) for extended source polarimetry. The reported [H18](#) values of MDCF and MDCPF (see their Table 5) refer to minimum surface brightness for a 4-sigma detection of a point source in 900 seconds on-source integration in Lissajous and chop-nod imaging and polarimetry scan modes, respectively.

Note that [H18](#) concedes that their reported values table is derived from limited observation of the dependence of sensitivity of HAWC+ detectors on line-of-sight (LOS) water vapor and aircraft altitude is not studied. However, ([Lopez-Rodriguez et al, 2022](#)) estimate that the OTFMAP polarimetric mode offered a reduction of observing overheads by a factor of 2.34 and an improvement in sensitivity by a factor of 1.80 when compared to the same on-source time polarimetric observations using the chopping and nodding mode. Based on the polarimetric observations in Survey of Extragalactic Magnetism with SOFIA (SALSA), they conclude that OTFMAP was a significant optimization of the polarimetric mode of HAWC+ and was quite cost effective as it increased the science collected per hour of observation up to an overall factor of 2.49.

3.3 DATA QUALITY CHARACTERISTICS OVER TIME

3.3.1 Full Width Half Maximum

Table 1 shows the Full Width Half Maximum (FWHM) of each bandpass as measured using Gaussian profiles, the finite size of the HAWC+ detectors, and a convolution across the measured filter bandpasses. As a way of monitoring the performance of the instrument the FWHM of calibrators (planets and asteroids) was measured multiple times in each band during all SOFIA/HAWC+ observing series. [Figure 5](#) shows the average measured FWHM for each band versus the SOFIA/HAWC+ observing series where the average is taken over multiple observations in the series and is a geometric mean of FWHM in X and FWHM in Y. As seen in the [Figure 5](#) the FWHM in each band was consistent and did not change much over the lifetime of HAWC+.

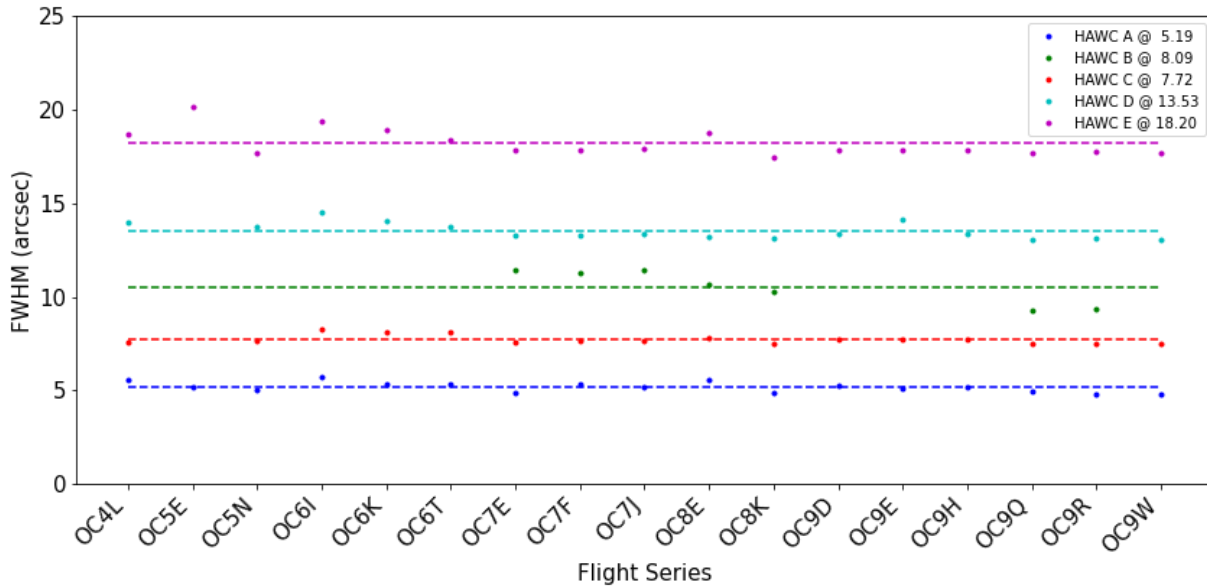


Figure 5 Measured beam full width half maximum (FWHM) by series. HAWC+ Band B data has been scaled by 1.3 in the figure for display purpose.

3.3.2 Flux Calibration Variability

The HAWC+ calibration procedure involved measuring fluxes of multiple calibrators (see Section 4.3 for details) in as many as possible combination of filters, observing mode (chop-nod and scanning), and observing configuration (imaging/total intensity and polarimetry) in each series. These fluxes were then used to derive the reference calibration factors as described in Section 4.3. To assess the variability of flux calibration over time the reference calibration factors for each source, HAWC+ filter, mode and configuration combination per observing series was averaged and compared to the average of the reference calibration factor (master calibration factor) for the entire lifetime of SOFIA.

The plots below show the percent difference between the reference calibration values (symbols) and the master calibration factors for each series and for each filter (colors) for both the polarimetry (

3. INSTRUMENT PERFORMANCE

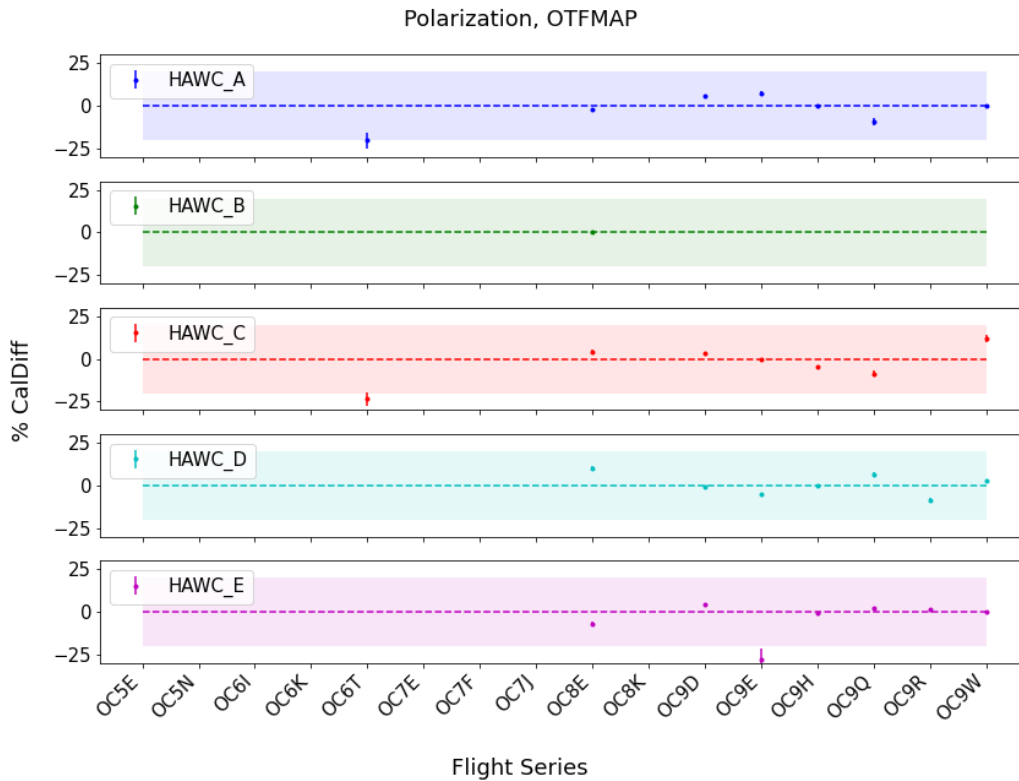
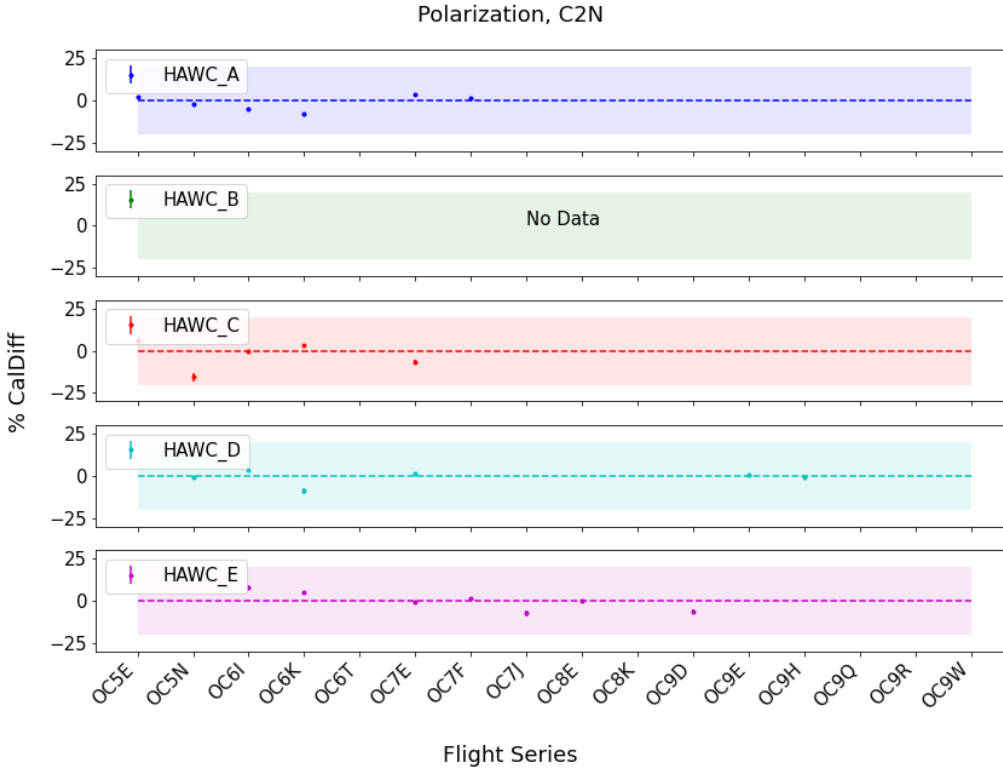
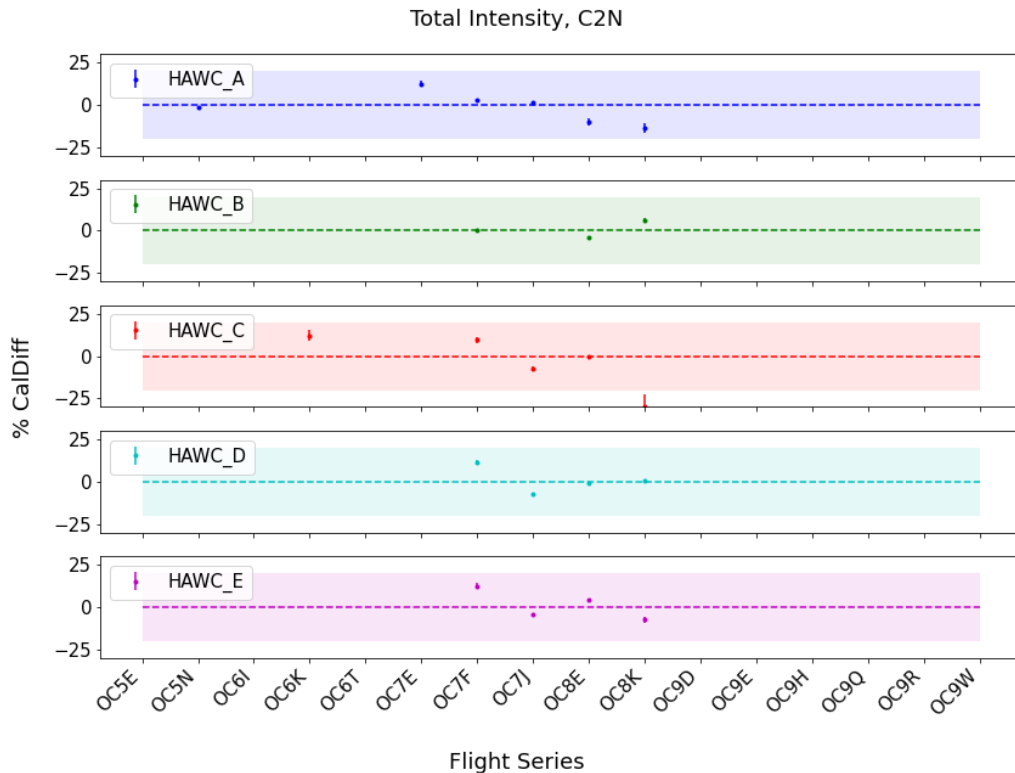


Figure 6 Trends in percent difference in the reference calibration factors for polarimetry data in the C2N and OTFMAP modes between each flight series and the average for the entire HAWC+ lifetime. The colored shaded region shows the nominal $\pm 20\%$ calibration requirement.



) and total intensity (imaging) modes (Figure 7). As seen in these plots, most of the series showed variations in reference calibration factors within 20% of the master calibration factor, a nominal requirement for the performance of the instrument. Observing series OC8K and OC9E showed reference calibration factors for a few long wavelength filters that were outside the nominal values. Due to the flight planning constrains the calibration observations for these two series were performed at a lower altitude (< 39,000 ft), resulting in higher water vapor overburden, which resulted in an off-nominal values of reference calibration factors in the longer wavelength band. Therefore, for these two series the master calibration factors were used to calibrate all science data. These reference calibration values are included in the SOFIA HAWC+ data reduction pipeline and is listed in Appendix B.

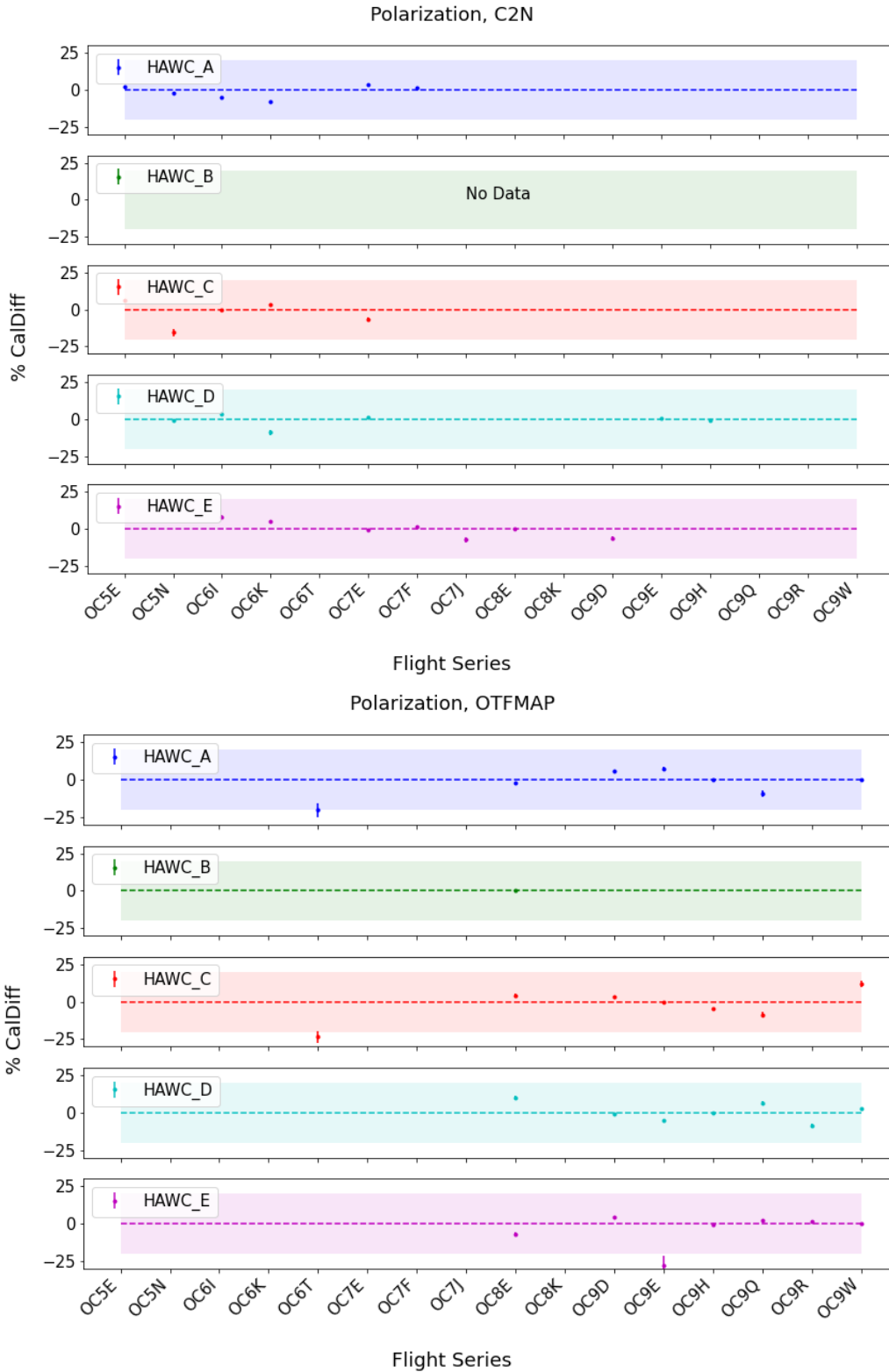


Figure 6 Trends in percent difference in the reference calibration factors for polarimetry data in the C2N and OTFMAP modes between each flight series and the average for the entire HAWC+ lifetime. The colored shaded region shows the nominal $\pm 20\%$ calibration requirement.

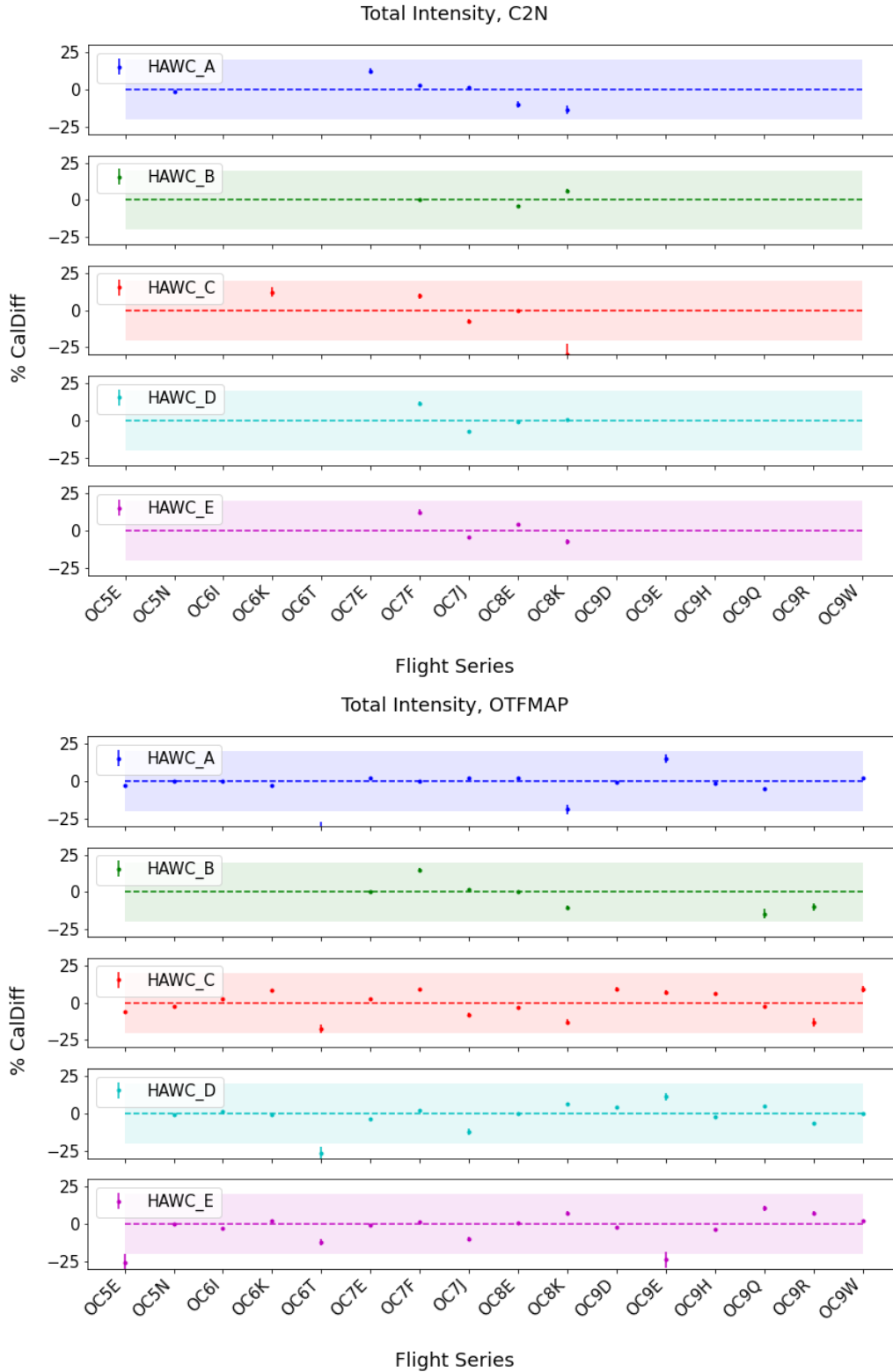


Figure 7 Trends in percent difference in the reference calibration factors for total intensity (imaging) data in the C2N and OTFMAP modes between each flight series and the average for the entire HAWC+ lifetime. The colored shaded region shows the nominal $\pm 20\%$ calibration requirement.

4. DATA

4.1 DATA PRODUCT & FORMAT

4.1.1 File Naming Conventions

Output files from the HAWC pipeline are named according to the convention:

$$\text{FILENAME} = \text{F}[\textit{flight}]_{\textit{HA}}[\textit{mode}]_{[\textit{aorid}]_{[\textit{spectel}]_{[\textit{type}]_{[\textit{fn1}[-\textit{fn2}]}}].\textit{fits}}$$

where *flight* is the SOFIA flight number, *HA* indicates the instrument (HAWC+), and *mode* is either *IMA* for imaging observations, *POL* for polarization observations, or *CAL* for diagnostic data. The *aorid* indicates the SOFIA program and observation number; *spectel* indicates the filter/band and the HWP setting. The *type* is a three-letter identifier for the pipeline product type, and *fn1* and *fn2* are the first and last raw file numbers that were combined to produce the output product. For example, a polarization map data product with AOR-ID 81_0131_04, derived from files 5 to 6 of flight 295, taken in band A with HWP in the A position would have the filename *F0295_HA_POL_81013104_HAWAHWPA_PMP_005-006.fits*. See the tables below for a list of all possible values for the three-letter product type.

4.1.2 Data Format

Most HAWC data is stored in FITS files, conforming to the FITS standard ([Pence, et. al., 2010](#)). Each FITS file contains a primary Header Data Unit (HDU) which may contain the most appropriate image data for that particular data reduction level. Most files have additional data stored in HDU image or table extensions. All keywords describing the file are in the header of the primary HDU (see Appendix [D](#) and [HAWC+ DRP User Manual](#)). Each HDU also has a minimal header and is identified by the EXTNAME header keyword. The algorithm descriptions in the user's manual give more information about the content of each extension.

4.1.3 Pipeline Products

The following tables list all intermediate and final products that may be generated by the HAWC pipeline, in the order in which they are produced for each mode. The product type is stored in the primary header, under the keyword PRODTYPE. By default, for Nod-Pol mode, the *demodulate*, *opacity*, *calibrate*, *merge*, and *polmap* products are saved and archived. For Chop-Nod mode, the *demodulate*, *opacity*, *merge*, and *calibrate* products are saved and archived. For Scan mode, the *scanmap* and *calibrate* products are saved and archived. For Scan-Pol mode, the *scanmappol*, *calibrate*, *merge*, and *polmap* products are saved and archived.

For polarization data, the pipeline also generates two auxiliary products: a polarization map image in PNG format, with polarization vectors plotted over the Stokes I image, and a polarization vector file in DS9 region format, for displaying with FITS images. These products are alternate representations of the data in the FINAL POL DATA table in the polarization map (PMP) FITS file. Similarly, for imaging data, a PNG quick-look preview image is generated as a final step in the pipeline. These auxiliary products may be distributed to observers separately from the FITS file products.

Data products that contain multiple AORs or that contain observations from multiple flights are referred to as multi-mission products. When multi-mission data are processed and stored in the database, they replace the corresponding single-mission/single-AOR data files. This process

usually results in fewer data files for a project. For HAWC+, the following data products can be multi-mission:

- imaging: *calibrate* (CAL)
- polarimetry: *merge* (MRG), *polmap* (PMP).

Table 3: Nod-Pol Mode Intermediate and Final Pipeline Data Products

Step	Description	PRODTYPE	PROCSTAT	Identifier	Saved*
Make Flat	Flat generated from Int. Cal file	obsflat	LEVEL_2	OFT	Y
Demodulate	Chops subtracted	demodulate	LEVEL_1	DMD	Y
Flat Correct	Flat field correction applied	flat	LEVEL_2	FLA	N
Align Arrays	R array shifted to T array	shift	LEVEL_2	SFT	N
Split Images	Data split by nod, HWP	split	LEVEL_2	SPL	N
Combine Images	Chop cycles combined	combine	LEVEL_2	CMB	N
Subtract Beams	Nod beams subtracted	nodpolsub	LEVEL_2	NPS	N
Compute Stokes	Stokes parameters calculated	stokes	LEVEL_2	STK	N
Update WCS	WCS added to header	wcs	LEVEL_2	WCS	N
Subtract IP	Instrumental polarization removed	ip	LEVEL_2	IPS	N
Rotate Coordinates	Polarization angle corrected to sky	rotate	LEVEL_2	ROT	N
Correct Opacity	Corrected for atmospheric opacity	opacity	LEVEL_2	OPC	Y
Calibrate Flux	Flux calibrated to physical units	calibrate	LEVEL_3	CAL	Y
Subtract Background	Residual background removed	bgssubtract	LEVEL_3	BGS	N
Bin Pixels	Pixels re-binned to increase S/N	binpixels	LEVEL_3	BIN	N
Merge Images	Dithers merged to a single map	merge	LEVEL_3	MRG	Y
Compute Vectors	Polarization vectors calculated	polmap	LEVEL_4	PMP	Y

Table 4: Chop-Nod Mode Intermediate and Final Pipeline Data Products

Step	Description	PRODTYPE	PROCSTAT	Identifier	Saved*
Make Flat	Flat generated from Int.Cal file	obsflat	LEVEL_2	OFT	Y
Demodulate	Chops subtracted	demodulate	LEVEL_1	DMD	Y
Flat Correct	Flat field correction applied	flat	LEVEL_2	FLA	N
Align Arrays	R array shifted to T array	shift	LEVEL_2	SFT	N

Step	Description	PRODTYPE	PROCSTAT	Identifier	Saved*
Split Images	Data split by nod, HWP	split	LEVEL_2	SPL	N
Combine Images	Chop cycles combined	combine	LEVEL_2	CMB	N
Subtract Beams	Nod beams subtracted	nodpolsub	LEVEL_2	NPS	N
Compute Stokes	Stokes parameters calculated	stokes	LEVEL_2	STK	N
Update WCS	WCS added to header	wcs	LEVEL_2	WCS	N
Correct Opacity	Corrected for atmospheric opacity	opacity	LEVEL_2	OPC	Y
Subtract Background	Residual background removed	bgssubtract	LEVEL_2	BGS	N
Bin Pixels	Pixels rebinned to increase S/N	binpixels	LEVEL_2	BIN	N
Merge Images	Dithers merged to single map	merge	LEVEL_2	MRG	Y
Calibrate Flux	Flux calibrated to physical units	calibrate	LEVEL_3	CAL	Y

Table 5: Scan Mode Intermediate and Final Pipeline Data Products

Step	Description	PRODTYPE	PROCSTAT	Identifier	Saved
Construct Scan Map	Source model iteratively derived	scanmap	LEVEL_2	SMP	Y
Calibrate Flux	Flux calibrated to physical units	calibrate	LEVEL_3	CAL	Y

Table 6: Scan-Pol Mode Intermediate and Final Pipeline Data Products

Step	Description	PRODTYPE	PROCSTAT	Identifier	Saved*
Construct Scan Map	Source model iteratively derived	scanmappol	LEVEL_2	SMP	Y
Compute Stokes	Stokes parameters calculated	stokes	LEVEL_2	STK	N
Subtract IP	Instrumental polarization removed	ip	LEVEL_2	IPS	N
Rotate Coordinates	Polarization angle corrected to sky	rotate	LEVEL_2	ROT	N
Calibrate Flux	Flux calibrated to physical units	calibrate	LEVEL_3	CAL	Y
Merge Images	HWP sets merged to single map	merge	LEVEL_3	MRG	Y
Compute Vectors	Polarization vectors calculated	polmap	LEVEL_4	PMP	Y

* The "saved" status denotes the default configuration in the pipeline for saving the intermediate data structures as it progresses from RAW to the final map. If the pipeline is run on RAW files, the 'Y' status products will be saved in their output directory.

4.2 CORRECTION FOR ATMOSPHERIC OPACITY

To combine images taken under differing atmospheric conditions, the pipeline corrects the flux in each individual file for the estimated atmospheric transmission during the observation, based on

the altitude and zenith angle at the time when the observation was obtained. Atmospheric transmission values in each HAWC+ filter have been computed for a range of telescope elevations and observatory altitudes (corresponding to a range of overhead precipitable water vapor values) using the ATRAN atmospheric modeling code, provided to the SOFIA program by Steve Lord. The ratio of the transmission at each altitude and zenith angle, relative to that at the reference altitude (41,000 feet) and reference zenith angle (45 degrees), has been calculated for each filter and fits with a low-order polynomial. The ratio appropriate for the altitude and zenith angle of each observation is calculated from the fit coefficients. The appropriate atmospheric models and the fit coefficient are included in the pipeline repository and the pipeline automatically applies this relative opacity correction factor directly to the flux in the Stokes *I*, *Q*, and *U* images, and propagates it into the corresponding error and covariance images.

4.3 FLUX CALIBRATION

The calibration factors are computed in a manner similar to that of another SOFIA instrument (FORCAST), taking into account that HAWC+ was a bolometer, not a photon-counting device. Measured photometry is compared to the theoretical fluxes of standards whose spectra are corrected as described in Section 4.2 above. The predicted fluxes in each HAWC+ passband are computed by multiplying the model spectrum by the overall response curve of the telescope and instrument system and integrating over the filter passband. For HAWC+, the standards used to date include Uranus, Neptune, Callisto, Ganymede, Ceres, Pallas, and Vesta. The models for Uranus and Neptune were obtained from the Herschel project (Müller et al. 2016) and the standard thermal models were used for the asteroids. All models were scaled to match the distances of the objects at the time of the observations. Calibration factors computed from these standards were then corrected by a color correction factor based on the mean and pivot wavelengths of each passband, such that the output flux in the calibrated data product was that of a nominal, flat spectrum source at the mean wavelength for the filter. Since the color correction as described above is tied to the reference altitude (41,000 feet) and reference zenith angle (45 degrees) these calibration factors are referred to as the reference calibration factor. See Appendix B for a table of those values and Appendix B of the FORCAST Archive User's Manual for more details on the process.

Raw calibration factors are computed as above by the pipeline, for any observation marked as a flux standard (OBSTYPE=STANDARD_FLUX) and are stored in the FITS headers of the output data product. The instrument team generally combined these factors across a flight series, to determine a robust average value for each instrument configuration and mode. The overall calibration thus determined is expected to be good to within about 10%.

For science observations, the series-average calibration factor was directly applied to the flux in each of the Stokes *I*, *Q*, and *U* images, and to their associated error and covariance images:

$$\begin{aligned}I' &= I/f \\Q' &= Q/f \\U' &= U/f \\ \sigma'_Q &= \sigma_Q/f\end{aligned}$$

$$\sigma'_{U} = \sigma_{U}/f$$

$$\sigma'_{QI} = \sigma_{QI}/f^2$$

$$\sigma'_{UI} = \sigma_{UI}/f^2$$

$$\sigma'_{QU} = \sigma_{QU}/f^2$$

where f is the reference calibration factor corrected to the observed altitude and zenith angle. The systematic error on f is not propagated into the error planes, but it is stored in the ERRCALF FITS header keyword. The calibration factor applied is stored in the CALFCTR keyword. Note that for Chop-Nod imaging data, this factor is applied after the merge step.

4.3.1 Instrumental Polarization

As with any polarization observations it is crucial to distinguish between the polarization caused by the telescope and instrument (instrumental polarization) versus that the intrinsic source polarization. HAWC+ employed three methods to determine the instrumental polarization (IP): i) observations of nominally unpolarized sources like planets and asteroids, ii) measurement of sources whose extended emission covers the full detector array covering large range of parallactic angles and iii) measurements taken during skydip, which are observation taken continually while scanning the telescope over a large range of zenith angles. Each of these methods have advantages and limitation. Using planets and asteroids to determine instrumental polarization measures only a small, central subset of pixels in the array, while using extended emission are very time consuming and do not uniformly sample all pixels. Even though skydip observation in not based on an astrophysical source, it measures all the pixel with high signal to noise and can be done in a reasonable amount of time. The specifics of each of these methods are already described in detail in [H18](#) and users are referred to that document. While observing standard source for flux calibration provided the instrumental polarization for free, the HAWC+ observing team performed multiple skydip observations during each flight and thus were able to derive instrumental polarization for the entire array for each flight/series. As with the flux calibration factors these instrumental polarization values are included in the pipeline and is automatically applied to all the polarization data.

4.3.2 Internal Calibrator:

HAWC+ controlled variations in detector responsivity by making measurements of its internal calibration source, which was a Boston Electronics IR-50 thin film thermal source. The source was square wave modulated at 3 Hz to provide a stable and repeatable infrared reference signal. Its purpose was twofold. The first was to correct for detector gain variations caused by changes in bias or background loading. The second was to determine the relative time constants of the detector pixels. These internal calibrator measurements, or INTCAL files, were typically 10–20 seconds in length, and the source was driven at a frequency of 3 Hz. INTCAL files were acquired before and after sets of four dithered polarimetry files and at other times as needed to calibrate scan data. See [H18](#) and [HAWC+ DRP User Manual](#) for further detail.

4.4 DATA ARTIFACT

Details can be found by clicking on SERIES or ISSUES to jump to specific sections within the following tables.

Table 7: List of Data Issues by HAWC+ Flight Series and Mission IDs

HAWC Series		
Series	Mission ID	Issues
OC4L	2016-12-01 HA F353	HAIMG_01 , HALISS_01a , HALISS_01b , HAPOL_01 , HAPOL_03 [FT355 Only]
	2016-12-03 HA F354	
	2016-12-06 HA F355	
	2016-12-08 HA F356	
	2016-12-09 HA F357	
	2016-12-14 HA F358	
	2016-12-15 HA F359	
	2016-12-16_HAF360	
OC5E	2017-05-11 HA F393	
	2017-05-12 HA F394	
	2017-05-13 HA F395	
	2017-05-17 HA F396	
	2017-05-18 HA F397	
OC5N	2017-10-17 HA F440	HAIMG_01 , HALISS_01a , HALISS_01b , HAPOL_01 , HAPOL_02
	2017-10-18 HA F441	
	2017-10-19 HA F442	
	2017-10-20 HA F443	
	2017-10-24 HA F444	
	2017-10-25 HA F445	
	2017-10-26 HA F446	
	2017-10-27 HA F447	
	2017-10-31 HA F448	
	2017-11-07 HA F449	
	2017-11-09 HA F450	
	2017-11-14 HA F451	
	2017-11-15 HA F452	
	2017-11-16 HA F453	
2017-11-17 HA F454		
OC9E	2021-11-03 HA F886	HALISS_01a , HALISS_01b , HAPOL_04
	2021-11-04 HA F887	
	2021-11-05 HA F888	
OC9Q	2022-06-01_HA_F879	HAPOL_05
	2022-06-02_HA_F880	
	2022-06-03_HA_F881	
	2022-06-04_HA_F882	
	2022-06-07_HA_F883	
	2022-06-09_HA_F884	
	2022-06-10_HA_F885	
	2022-06-11_HA_F886	
OC9R	2022-06-21_HA_F889	HAPOL_05
	2022-06-23_HA_F890	
	2022-06-27_HA_F891	
	2022-06-30_HA_F892	
	2022-07-03_HA_F893	
	2022-07-05_HA_F894	
	2022-07-06_HA_F895	

OC9W	2022-09-21_HA_F916 2022-09-22_HA_F917 2022-09-23_HA_F918 2022-09-27_HA_F919 2022-09-28_HA_F920 2022-09-29_HA_F921	HAPOL_05
------	--	--------------------------

Table 8: Details of the Known Data Issues for HAWC+

Mode	Issues	Series
Lissajous Polarimetry	[HALISS_01a] Dark Outlines: When observing very bright extended sources with little sky background, dark areas appear to outline the bright emission.	All
	[HALISS_01b] Low Scan Velocity Bleed Through: Occasionally artifacts seen as dark regions off-source or dark spots appear on the array due to insufficient mapping coverage.	All
Imaging	[HAIMG_01] Ghosting: Streaks and false sources in data due to very bright targets, can resemble chop smear.	OC4L , OC5E , OC5N
Polarimetry	[HAPOL_01] Chop Smear: Smearing due to observations being taken while chopping secondary still moving, causing streaking and false sources above and below bright objects.	OC5E , OC5N
	[HAPOL_02] Nod Misalignment: A mechanical issue associated with the telescope has resulted in misalignment or imperfect matching of the Nods in HAWC Chop-Nod mode (C2N(NMC)) mode with large Nod Throws ≥ 120 arcsec). This has resulted in double sources with misalignments on scales greater than 3 arcsec (more at larger Nod Throws). This primarily affects polarimetry mode where Chopping and Nodding are used rather than a Lissajous pattern.	OC4L , OC5E , OC5N
	[HAPOL_03] Helium Contamination: Helium contamination on the detector caused time variable phase shifts of ~ 30 degrees at 10 Hz. This only occurred on 2016-12-06 HA F355.	OC4L [FT355 only]
	[HAPOL_04] Flux Calibration: This series had a few cancelled and postponed flights resulting in low numbers of standard star observations and all observations below altitude of 39K. This resulted in reference flux calibration values that were considerably off compared to the historic data. Therefore, this series has been calibrated with an average value derived from historic data.	OC9E
	[HAPOL_05] High Temperature: HAWC+ cooling current consumption rate had increased dramatically after the repair of the instrument which resulted in shortening the flight duration and still losing parts or all of the last legs of some flights. To elongate the hold time, parts or all of polarimetric observation for a number of targets were acquired at higher temperature than the nominal 0.17K. The planned calibration at higher temperature was not possible before the end of the program and as a result, the polarization observations at 0.225K are deemed unreliable.	OC9Q [F883 only], OC9R [F892 only], OC9W [F919, F921 only]

4.5 KNOWN ARTIFACTS & MITIGATION

4.5.1 Dark outline around an extended emission

Significance: The first artifact described here (HALISS_01a) is from [Table 8](#). [Figure 8](#) shows an example observation of a bright extended emission that has a lot of negative flux values around the extended emission that appear dark in the displayed image. This is the result of the OTFMAP that is small compared to the source that is being observed and thus has no “true” background emission-free region in the FOV. Such cases result in improper estimation of the background emission and an overcorrection of backgrounds in the entire frame.

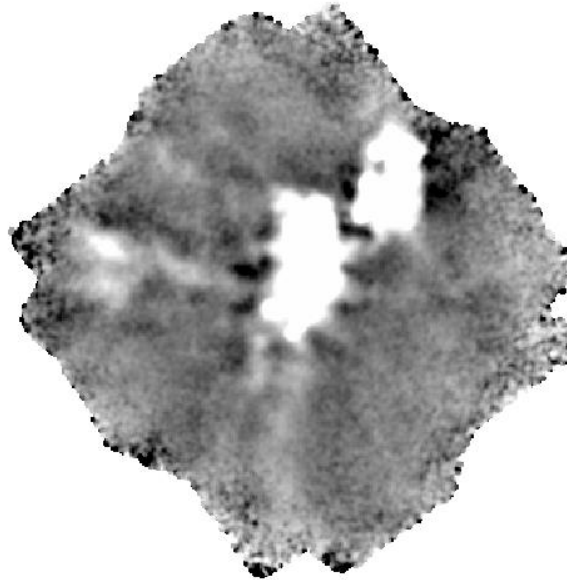


Figure 8 *Observation of a bright extended source showing dark (negative flux values) outline around the extended emission.*

Fix: The DPS team investigated this issue and implemented a solution for data acquired after Cycle 7, where the lowest negative pixels in each of the R and T array are added to the entire data and the nominal pipeline reduction is performed. If this artifact is found in data that was acquired before Cycle 7 and not re-processed, then `qubgsubtract` needs to be set to true in the background subtraction module to implement this solution for the data. Note that this solution does not work in every case and data should be checked carefully to ensure there are no anomalous polarization values in the maps.

4.5.2 Low Scan Velocity Bleed Through

Significance: This artifact is usually seen in a set of scans, but it does not appear in each of the individual scans. This is probably because of the variations in the background emission which changes the overall levels of the flux seen by the bolometers. This artifact looks like a series of bad pixels along the scan direction, as shown below in [Figure 9](#).

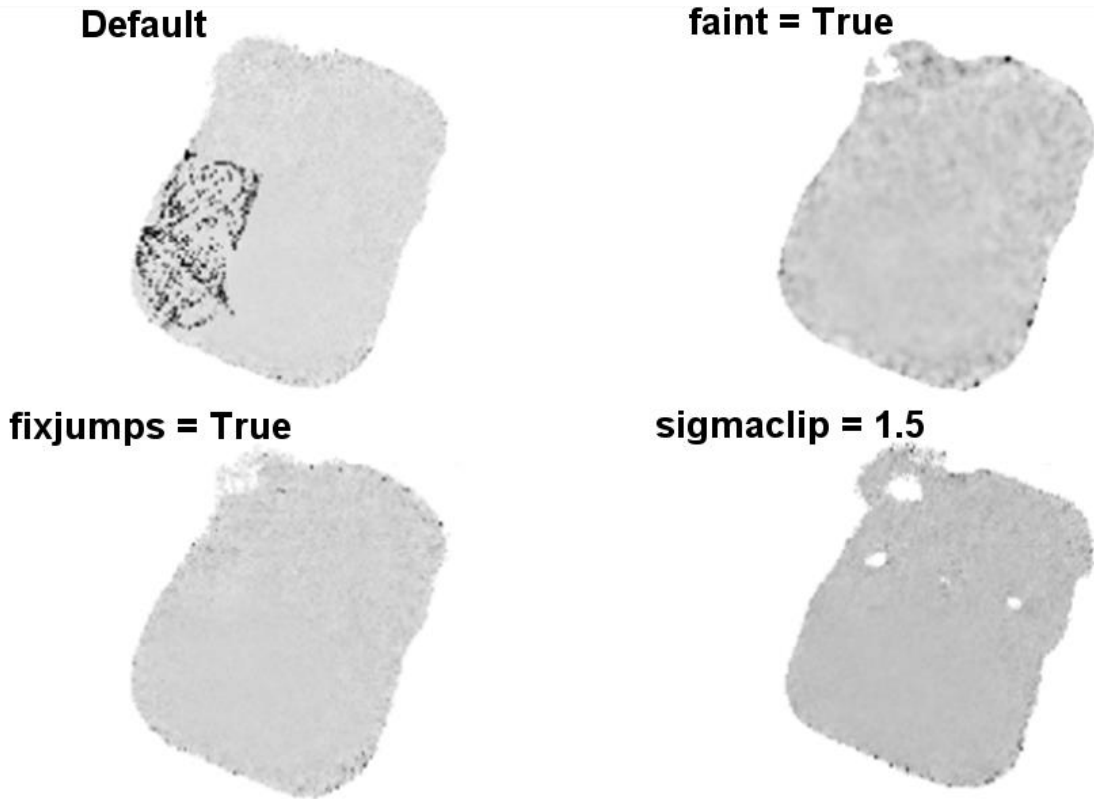


Figure 9 (Top Left) Example of a low scan velocity bleed through. (Top Right) Example of a data product using faint flag that results in mitigation of low scan velocity bleed through. (Bottom Left) Example of a data product using fixjumps flag that results in mitigation of low scan velocity bleed through. (Bottom Right) Example of a data product using sigmaclip flag that results in mitigation of low scan velocity bleed through.

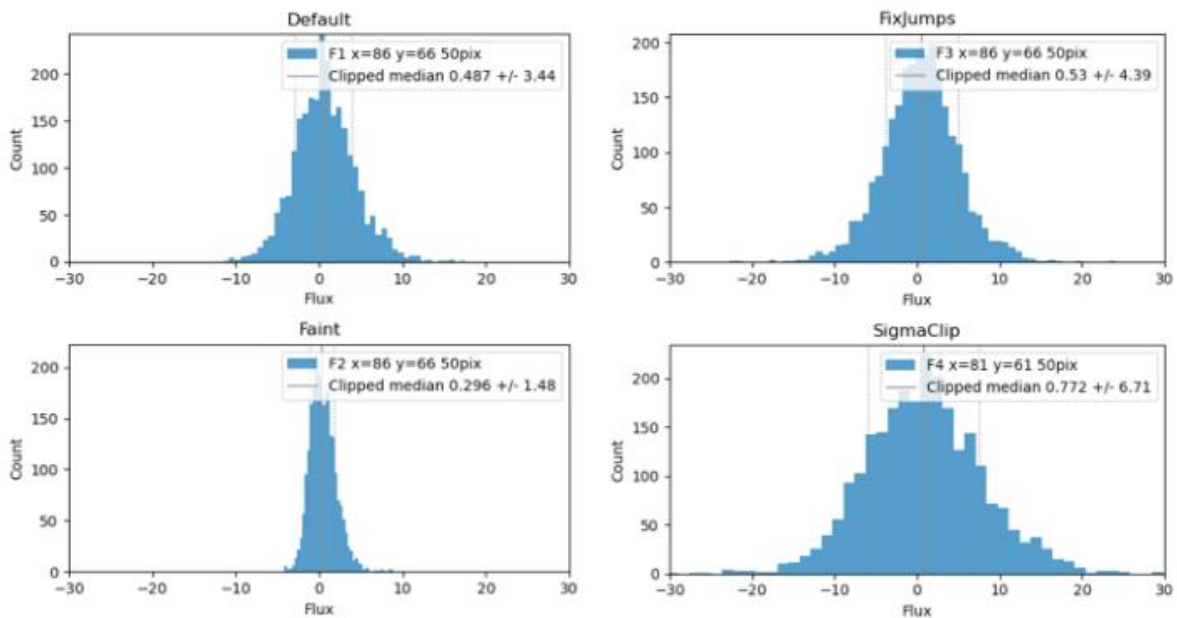


Figure 10 Histogram of the pixel values in a 50-pixel radius around the boresight in [Figure 9](#).

Fix: There are several ways this artifact can be mitigated, and the method used may depend on the source and the background emission. If the source is faint, then the faint flag in the pipeline can be used, which will aggressively filter the background to enhance the source emission (see [Figure 9](#) and [Figure 10](#)). This flag should be used with caution since its use will produce large noise in the background. This flag may work with point sources but not extended emission.

The other flag used to mitigate this artifact is reducing the value of sigma clip, as shown in [Figure 9](#) and [Figure 10](#) used in the pipeline (default = 5) which removes the frames that are outside of the permissible scanning speed range by iteratively removing speeds that are n times the standard deviation away from the median speed value.

The last flag used to mitigate this artifact is fix jump, which attempts to ‘fix’ residual flux jumps that result from imprecise correction in the MCE. Long jumps are re-levelled, while shorter ones are flagged out to minimize impact on source structure, as shown in the examples in [Figure 9](#) and [Figure 10](#).

4.5.3 Low CentroidExpMsec

Significance: All of the raw HAWC+ data is stored as timestream, and the pipeline constructs the different chops/nods by choosing the “good” data using various data cuts, one of which is to monitor the peak flux value of a bolometer in the HAWC+ array. After the demodulate step in the pipeline, a demodulate plot (DPL) is produced, which can be used to check the results of the demodulate step. In some cases where the load on the bolometer varies, as can be seen below in [Figure 11](#), the peak flux value in the given bolometer can drop to very low values, resulting in this part of the data being excluded by the pipeline. In the [Figure 11](#), green represents the data that is included in the map generation and white is excluded.

Fix: This issue can be fixed by changing the default value of tracking tolerance in the demodulate step of the pipeline. The track_tol value in the demodulate step will use this number as the tracking tolerance in arcseconds. Samples with tracking deviation larger than this number will be rejected. If set to ‘beam’, the beam size for the filter band will be used. If set to ‘centroidexp’, the CentroidExpMsec data stream will be used to flag data, rather than the TrackErrAoi3/4 data stream. Setting it to -1 will turn off tracking rejection entirely. The default is centroidexp. RHS of [Figure 11](#) shows the DPL plot where track_tol has been used to ‘beam’ instead of the default ‘centroidexp’, resulting in inclusion of all the chop/nod data in the map generation.

Note that if this setting is used to reduced C2N data in polarimetry mode then each extension in the final data should be carefully checked to ensure that including all the timestream in the reduction does not create any artifacts in the polarization data, especially debias percent polarization, polarization angle, and flux as show in the examples below ([Figure 12](#) to [Figure 15](#)).

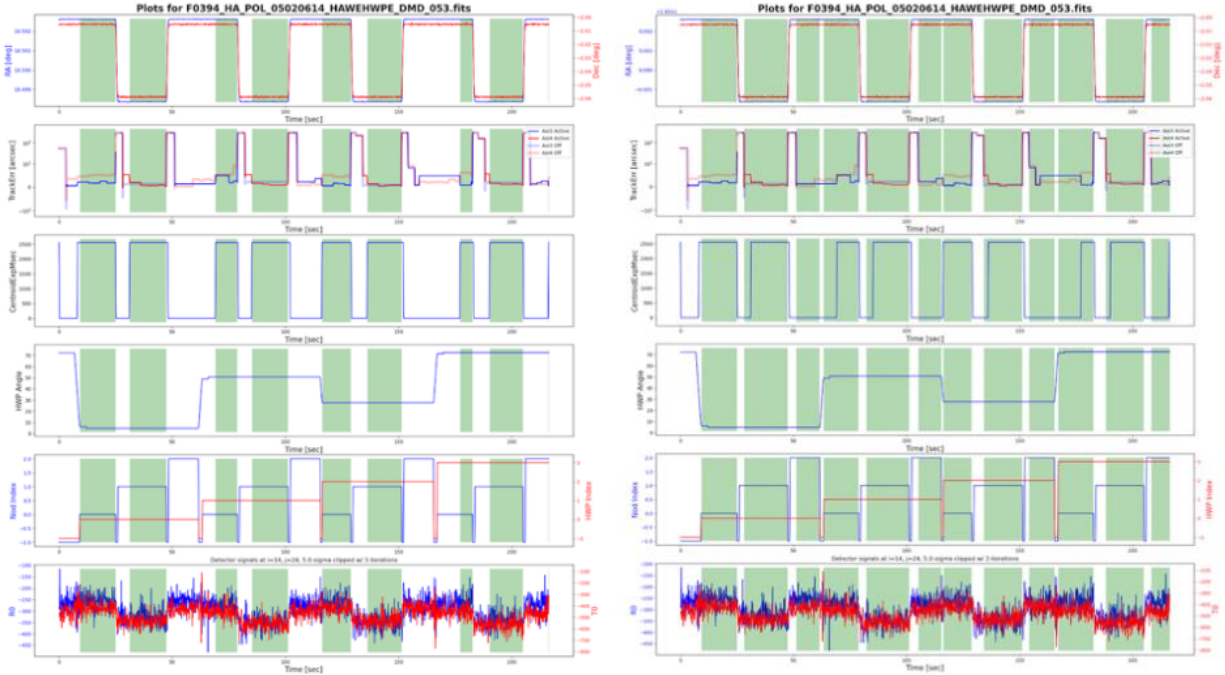


Figure 11 (Left) Example DPL plot showing the centroid value (third panel from the top) falling down to a very low number in the middle of a chop/nod cycle, which results in exclusion of the data in this part of the time stream. (Right) Example DPL plot showing the inclusion of the data in the time stream when track tolerance is set to beam instead of centroid.

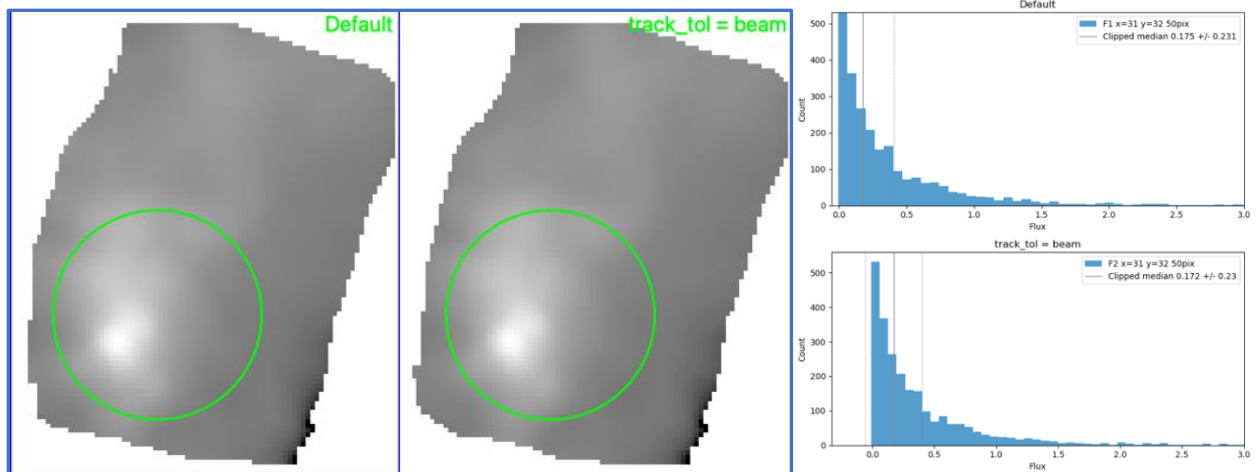


Figure 12 (Left) Low centroid artifact Stokes I before and after setting track_tol to beam. (Right) This histogram is the data from the green circle in the LHS panel, showing that the clipped median of the two histograms are well within the uncertainty in each case.

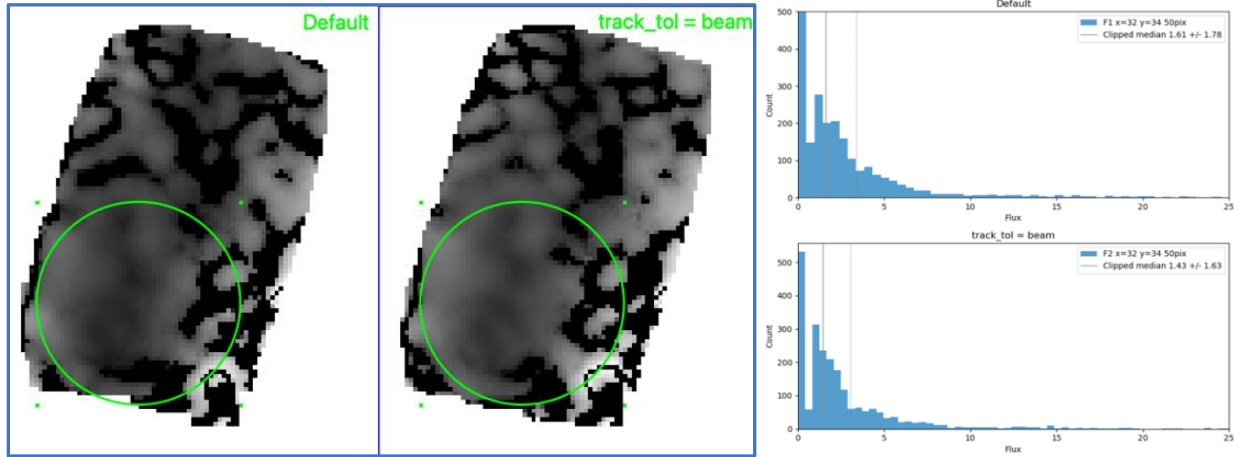


Figure 13 (Left) Low centroid artifact, Detbias % Pol before and after setting track_tol to beam.

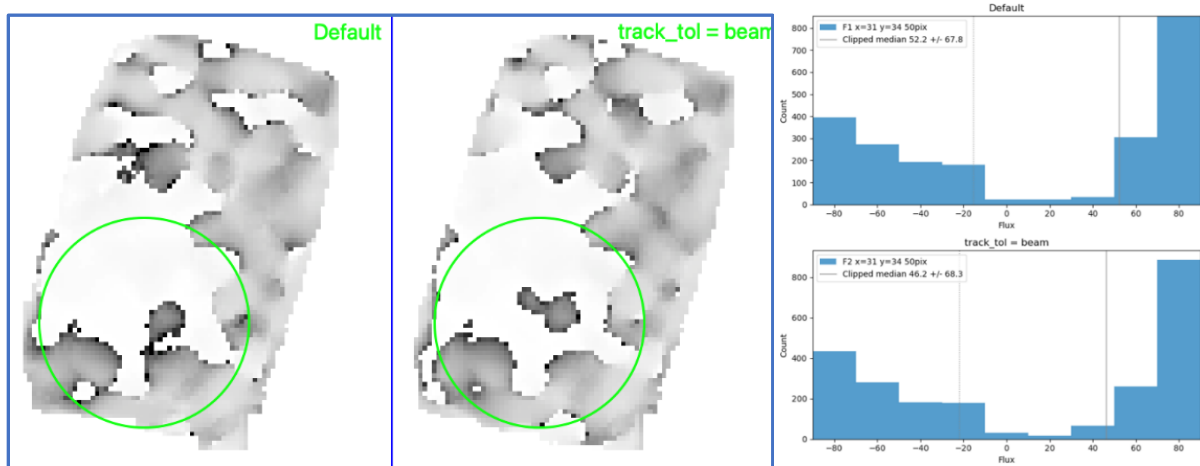


Figure 14 (Left) Low centroid artifact, Rotated Pol angle before and after setting track_tol to beam.

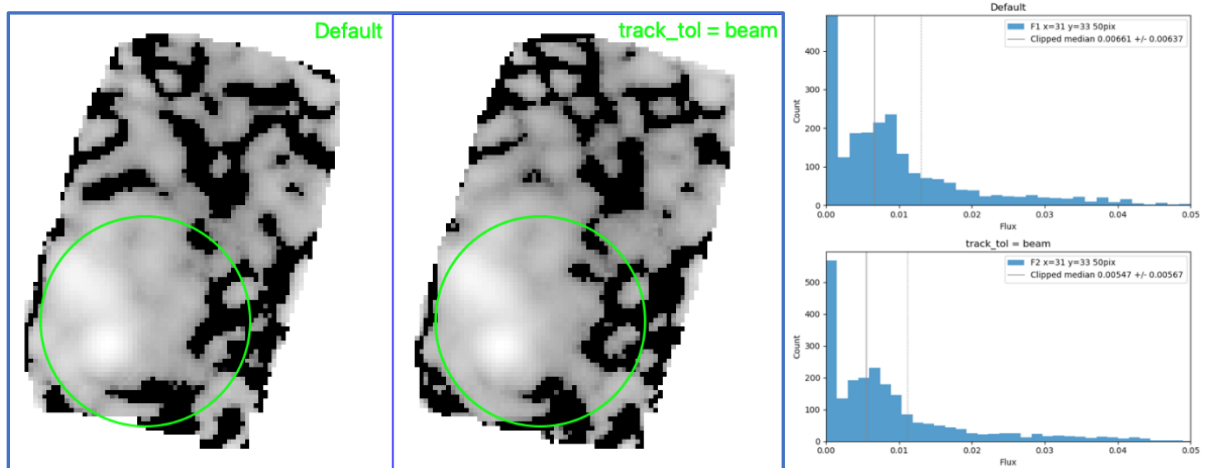


Figure 15 Low centroid artifact, debias pol flux before and after setting track_tol to beam.

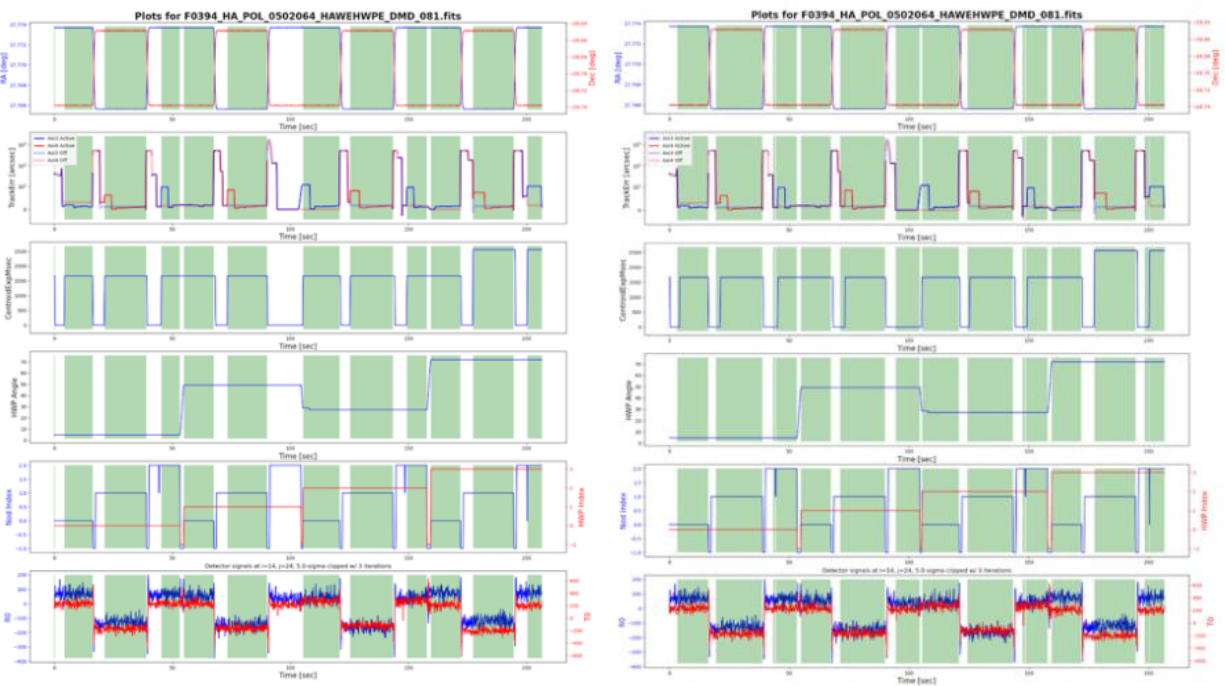


Figure 16 Characteristics of Tracking Error I.

4.5.4 Tracking Error I

Significance: Telescope tracking in the C2N mode can be diagnosed using [Figure 16](#), left hand side, second panel from the top, which shows the AOIs that were active during different chop/nod cycles. As seen in [Figure 16](#), during data collection in Nod A, HWP 2, the AOI lost tracking and went into a high state. The track star was recovered soon after and the AOI was then in a nominal state. This resulted in the pipeline excluding the time series for Nod A, HAW 2. Examination of raw data shows that even though AOI 3 was in a high state for a brief period the fluxes in the bolometer did not vary by much. Note that the example shown in [Figure 16](#) may also be related to the artifact described in [Section 4.5.3](#).

Fix: The mitigation in this case is the same as the one in [Section 4.5.3](#), i.e., by setting the track tolerance to beam the pipeline can be forced to include data in Nod A, HWP 2 and reduce the data with a full set of Chop/Nod and HWPs as shown in the RHS panel of [Figure 16](#).

4.5.5 Tracking Error II

Significance: [Figure 17](#) shows various cases where tracking while collecting C2N data has failed. In the first case, top left hand side of [Figure 17](#) the tracking fails while taking the data in HWP 3 and the AOI 3 goes in a high state. While the top right hand side and the bottom panel of [Figure 17](#) show that the AOI 3 was in a nominal state during the entire C2N observations, AOI 4 was always in an off-nominal state.

Fix: Unfortunately, in this case there is no mitigation, and the pipeline excludes these files from processing. In such cases the intermediate files should be carefully checked to make sure that the

pipeline has indeed excluded these files. Here it can be seen that there is a DMD file but no corresponding OPC and CAL files.

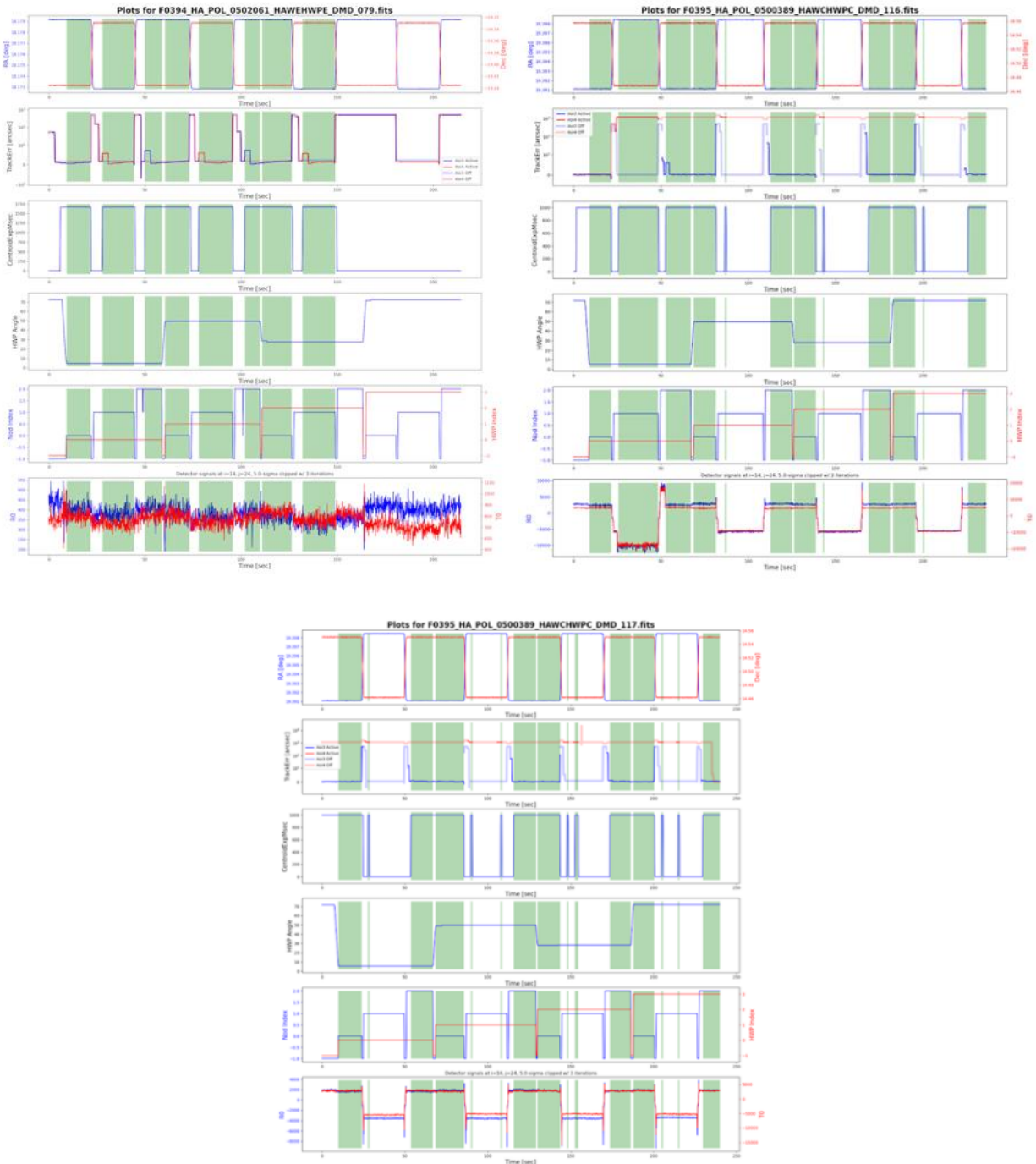


Figure 17 Characteristics of Tracking error II.

4.5.6 Incomplete HWP

Significance: Figure 18 shows a case where a C2N observation was done in only 2 HWP angles (see second last panel from the bottom in Figure 1818) and not the whole set of 4 HWP angles. This could be due to the observations being aborted because of some observing issue or the control software hitting an error state.

Fix: These cases (data files) where there are no observations in a full set of HWP angles should be excluded from processing. As in the previous case, the intermediate files should be checked to ensure there are DMD files but no OPC and CAL files.

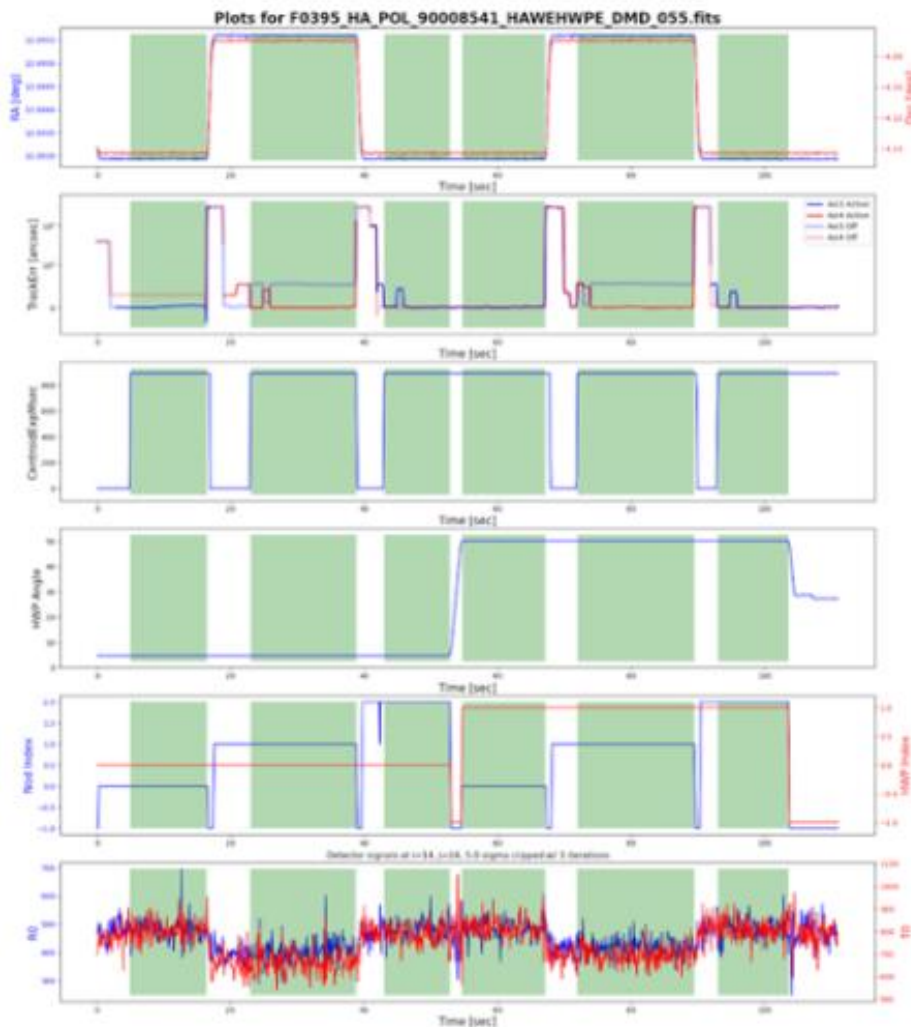


Figure 18 Characteristics of incomplete HWP.

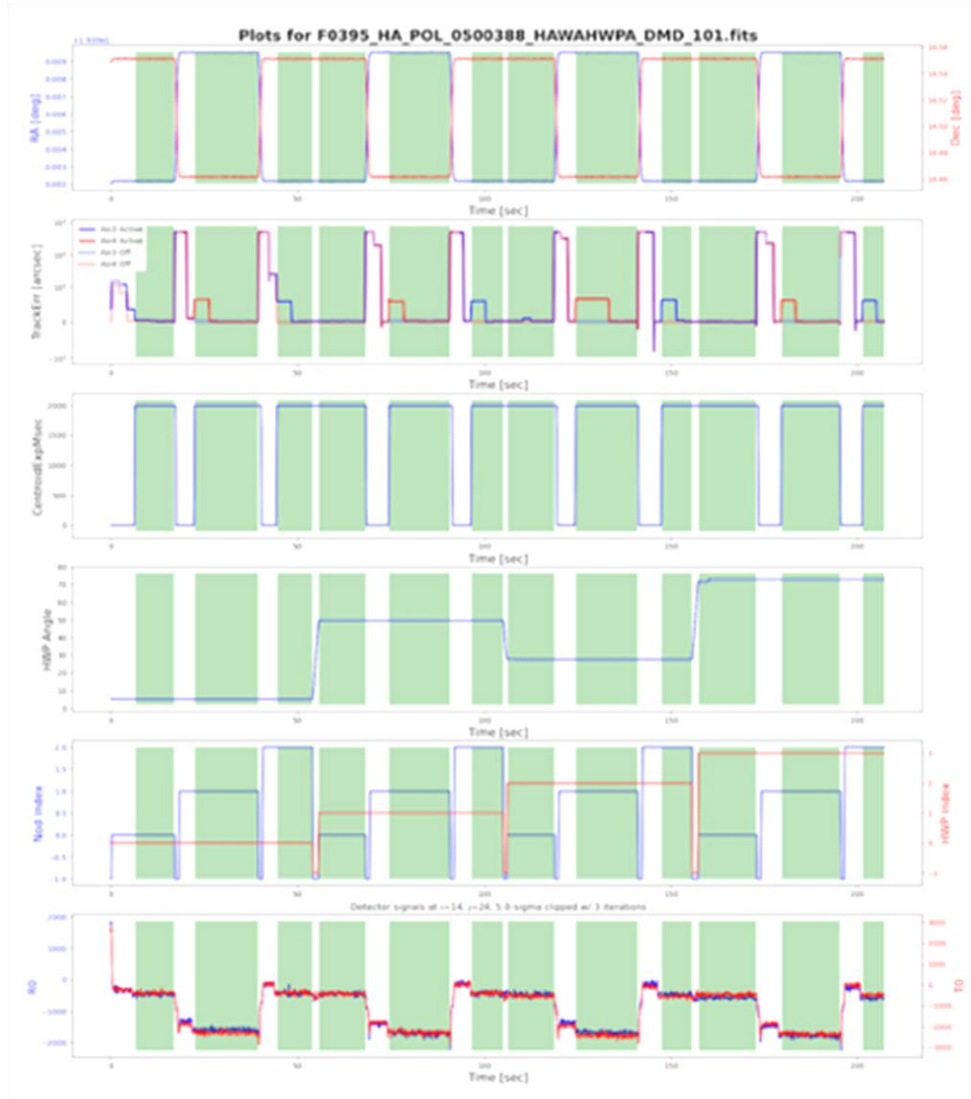


Figure 19 Characteristics of URD Vignetting.

4.5.7 URD Vignetting

Significance: Vignetting by the observatory upper rigid door (URD) causes large, occasional excursions in time series signals which, due to the serial approach to measuring polarization, end up corrupting the polarization measurements. The characteristics of vignetting can be seen in several ways where anomalous, correlated polarization vectors will be found in the output map. For infrequent vignetting, this can often be confirmed with outlier means and often gradients in the Stokes I image, and larger values in the uncertainty image. Anomalous values and uncertainties in one of the Stokes Q or U images may also be noticed. The pipeline QA diagnostic plots (DPL) calculate the Stokes I variance to flag candidate URD vignetting events, in particular, the ratio of “real” variance (in phase with chopper) to “imaginary” as listed on the top of the DPL plot in [Figure 19](#). Values greater than 2 signify that there is probably a vignetting event during one or more of the chop/nod cycles.

Fix: Observations with known URD vignetting should be excluded from processing but individual OPC and CAL vignetted files should be checked and compared with non-vignetted data to see if the data is salvageable.

4.5.8 Double Source

Significance: As can be seen from the screen shot below, the WCS registration of the standard observation, Neptune, has failed and two sources can be seen in the image. From the infiles.txt, it can be seen that there are only two input files, 073 and 087. Querying the JPL Horizons database, it can be confirmed that file 073 has the correct WCS and 087 has an offset.

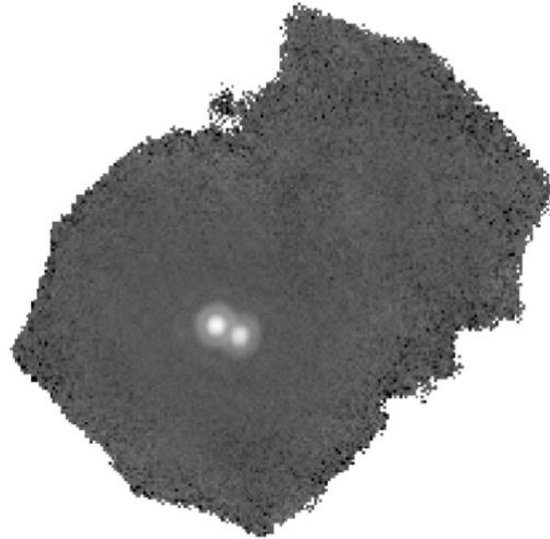


Figure 20 Characteristics of double source.

Run only two modules

```
config=default.cfg
[conditionals]
[[fits.OBS_ID=2017-10-17_HA_F440-90_0083_14-073]]
  unlock=pointing
  pointing=0,0
  lock=pointing

[[fits.OBS_ID=2017-10-17_HA_F440-90_0083_14-087]]
  unlock=pointing
  pointing=0,0
  lock=pointing
```

Figure 21 zero_Pointing.cfg.

```
recipe=checkhead, scanmap
[scanmap]
  options="config=/dps/preview/2017-10-17_HA_F440/12476-img_SDS/g6/pointing/zero_pointing.cfg"
# options="config=/dps/preview/2017-10-17_HA_F440/12476-img_SDS/g6/pointing/pointing_correction.cfg"
```

Need the fullpath to zero_pointing.cfg

Figure 22 man_Reduc.cfg For Zero Pointing Part I.

Fix: Since this observation is of point source, the pipeline can be used to fix the WCS issue. The pipeline will need to be run twice, once by setting the pointing offset to zero so that the pipeline can figure out what the offsets are and then running the pipeline with the offsets found in the previous step.

Configuration file for Zero Offset: The two configuration files, `zero_pointing.cfg` (Figure 21) and `man_reduc.cfg` (Figure 22), need to be generated, then run the pipeline.

Run the pipeline:

```
% reduc_pipe -c man_reduc.cfg -o pointing infiles.txt
```

Look for the following output (Figure 23):

```
2023-02-08 16:50:26,430 - sofia_redux.scan.reduction.reduction - INFO - [Source] (check) (exposureclip) (sync)
2023-02-08 16:50:29,171 - sofia_redux.scan.scan.scan - INFO - Instant Focus Results for Scan 2017-10-17_HA_F440-90_0083_14-073:
Asymmetry: x = -19.656% +- 0.056%, y = 42.969% +- 0.056%
Elongation: -0.400%

2023-02-08 16:50:29,212 - sofia_redux.scan.scan.scan - INFO - Pointing Results for Scan 2017-10-17_HA_F440-90_0083_14-073:

Peak: 4156466.29377 (S/N ~ 248.76669)
Integral: 4765359.1789 +- 19155.9375
FWHM: 8.3518 +- 0.0498 (arcsec)
(a=9.735209+-0.050935 arcsec, b=7.164985+-0.050935 arcsec, angle=86.701060 deg)
Offset: 6.248 arcsec, -12.250 arcsec (dAZ, dEL)

SIBS offset --> 1.7892, -2.8198 pixels
2023-02-08 16:50:29,219 - sofia_redux.scan.scan.scan - INFO - Instant Focus Results for Scan 2017-10-17_HA_F440-90_0083_14-087:
Asymmetry: x = 8.906% +- 0.047%, y = -17.824% +- 0.047%
Elongation: 1.660%

2023-02-08 16:50:29,258 - sofia_redux.scan.scan.scan - INFO - Pointing Results for Scan 2017-10-17_HA_F440-90_0083_14-087:

Peak: 2215622.44232 (S/N ~ 357.02513)
Integral: 2283435.4713 +- 6395.7276
FWHM: 7.9185 +- 0.0330 (arcsec)
(a=8.149457+-0.033093 arcsec, b=7.694023+-0.033093 arcsec, angle=69.875819 deg)
Offset: -1.782 arcsec, 4.404 arcsec (dAZ, dEL)

SIBS offset --> -0.1555, 1.3357 pixels
2023-02-08 16:50:29,259 - sofia_redux.scan.reduction.reduction - INFO - Reduction complete! (46.886 seconds)
2023-02-08 16:50:29,259 - sofia_redux.scan.reduction.reduction - DEBUG - Total reduction time = 75.559 seconds.
2023-02-08 16:50:29,260 - sofia_redux.instruments.hawc.stepparent - DEBUG - GetArg: from arg list, done (noout=False)
2023-02-08 16:50:29,268 - sofia_redux.instruments.hawc.dataparent - DEBUG - User config file: /dps/pipelines/hawc/hawcdrp/3.2.0/hawc/
```

Figure 23 Output of Part I.

Use the offset (dAZ, dEL) found in the log (see Figure 23) in a new pointing config file and run the pipeline.

```
config=default.cfg

[conditionals]
[[fits.OBS_ID=2017-10-17_HA_F440-90_0083_14-073]]
unlock=pointing
pointing=6.248,-12.250
lock=pointing

[[fits.OBS_ID=2017-10-17_HA_F440-90_0083_14-087]]
unlock=pointing
pointing=-1.782,4.404
lock=pointing
```

Figure 24 `pointing_correction.cfg`, Part II.

```

recipe=checkhead,scanmap
[scanmap]
# options="config=/dps/preview/2017-10-17_HA_F440/12476-img_SDS/g6/pointing/zero_pointing.cfg"
options="config=/dps/preview/2017-10-17_HA_F440/12476-img_SDS/g6/pointing/pointing_correction.cfg"

```

Use the new pointing offset file

Figure 25 *man_reduc.cfg* for Part II.

Run the pipeline (see Figure 25):

```
% redux_pipe -c man_reduc.cfg -o pointing infile.txt
```

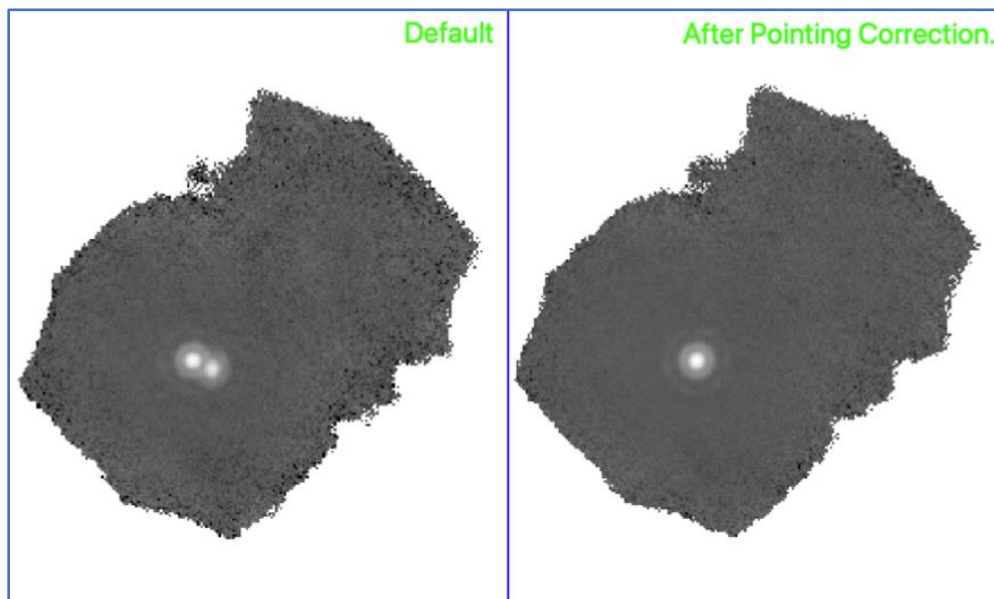


Figure 26 *Before and after pointing correction.*

Finally, run the pipeline again to calibrate the SMP file generated above.

```
% redux_pipe -o pointing pointing/*SMP*
```

The product of this pipeline run, with before and after images, is shown in Figure 26.

4.5.9 “Peanut” PSF

Significance: Some of this artifact is seen in the standard observation; the PSF looks like a peanut. This artifact was observed on flights between May and November of 2017 and was due to 0.7-degree rotational misalignment between chop and nod displacement.

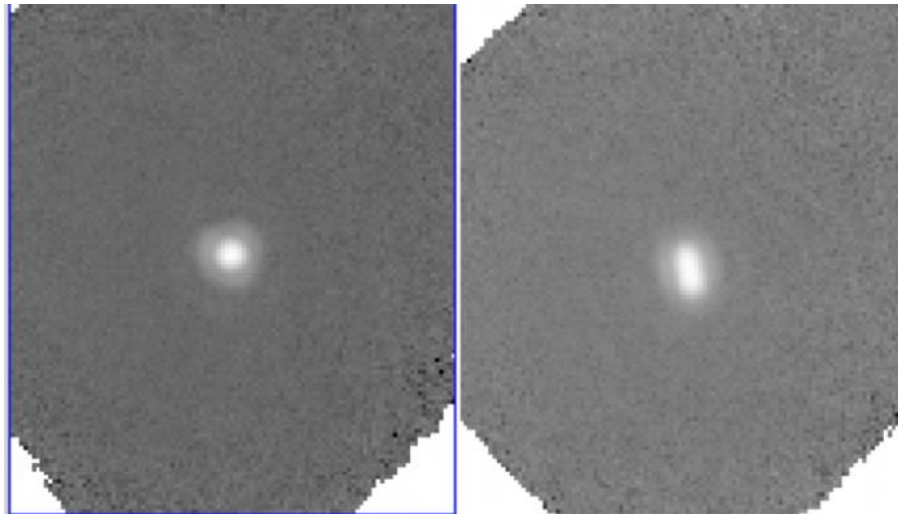


Figure 27 *Characteristics of peanut PSF.*

Fix: In the above example (Figure 27) there are two files, 080 and 081, where 080 had no misalignment and 081 has a chop nod misalignment. Since there is no mitigation for this issue, the bad file is excluded, and a note is made in the QA comments.

4.6 AN EXAMPLE OF BASIC POLARIZATION DATA INSPECTION AND VISUALIZATION

The notebook provides a walk-through of the steps of looking into the content and further calculation and visualization:

https://github.com/SOFIAObservatory/Recipes/blob/master/HAWC_30Dor.ipynb

4.7 OBSERVATIONS AT HIGHER TEMPERATURE

There is a relatively small subset of imaging and polarization observations for a few science targets on IRSA. The “High Temperature” refers to the set temperature for HAWC+ detectors (0.225K as opposed to the nominal 0.17K). Increase in the operational temperature for bolometers changes the detector gain and their bias. The degree of these changes is temperature dependent. The very idea of observation at higher temperature originated from the notion that the cooling current for the detectors could last longer if the bolometers were kept at higher temperature than 0.17K. Increasing the temperature up to >0.2K showed a significant effect in elongating the observation by preserving the cooling current (a.k.a, ADR current).

For these off-nominal data, all the tuned bias curves for detectors in each subarray had to be examined and a new flat frame (sky flat) and bad pixel mask had to be constructed from the data and the internal calibration data taken at the same temperature. The condition and characterization of this sky flat determined the possibility of appropriate treatment of the reduced data. The scheduled end of the SOFIA program in 2022 imposed harder constraint on the already tight schedule of HAWC+ observations over a much shorter time for completing the highest priority observations. This time limit prevented many planned calibration observations at higher

temperatures, which in turn jeopardized the chance of proper reduction for high temperature data for some projects.

The reprocessing effort of Cycle 5 to Cycle 9 data may result in creating appropriate sky flats to be used for reducing these data. When downloading the data for these targets, ensure that the portion of data from these listed flights is treated separately from the data taken at nominal temperature.

Table 9: Data Taken with Higher Detector Temperature

F883	NGC4631 NGC2276	D/D D/Open	NGC2276 [Fadda et al target] has nominal temp observations at both requested bands at nominal temp
F892	BYF77 Fil8	D/D E/E	BYF77 observations included 7 pointings (09_0048_45,46,47,48, 49, 50, 51) all observed at high temp - intcal 073 is taken at high temp
F895	BYF77	D/D	All the pointings of BYF in this flight was also observed at high temp
F916	IRAS 00450+7401	A/Open	
F919	Orion bar	A/A	Orion bar has observation at nominal temp in F686, F919
F921	Cep_L1157	E/E	There are nominal temp data for this target

5. SCIENTIFIC RESULTS

5.1 EXTENDED SOURCE POLARIMETRY

HAWC+ polarimetry mode was used to create large continuous maps of extended sources such as intergalactic filaments, giant molecular clouds, and the galactic plane, as part of various legacy programs. In a few projects such as scanning the galactic plane, to cover those vast areas with optimum number of overlapping mosaics, the scanning characteristics such as speed and amplitude were pushed to the maximum feasible limit that ensured quality data. The increased amplitude was essential to include a reasonable off-source region in each mosaic and measure background radiation.

It should be noted that for these custom-designed large mosaic mappings, it was possible that the standard calibration approach would fail to characterize the total and polarized fluxes and their inferences on the magnetic field alignment and strength, and therefore a custom calibration process was deemed essential. As of completion of this document, the investigative science team has not reached that conclusion. Please refer to the associated publications of each data set for an accurate description of the calibration steps of large scans.

HAWC+ data from Cycle 5 to 9 have been reprocessed using the latest, more mature version of the pipeline, and several fixes such as correction for the extended emission are embedded into the code, which resulted in a number of historically known artifacts being mitigated (see details in Sections 4.4 and 4.5). However, there could be data sets, especially for extended sources where the reduced data passed basic qualification and were labeled as “NOMINAL”, that were still not used in the associated scientific publication for the project. Therefore, a careful comparison of the configuration parameters used by the legacy teams to the publicly available pipeline should be made if legacy data is to be used for further science.

5.2 HAWC LEGACY SURVEYS

The legacy programs for imaging and polarimetry with HAWC+ are listed below with a summary of their science objectives, project websites, and publications. With this provided information, the fully public data on IRSA can be accessed for other defined projects.

5.2.1 FIELDMAPS: Filaments Extremely Long and Dark: A Magnetic Polarization Survey

- Principal Investigator: *Ian Stephens (Worcester State University)*
- Plan ID: 08_0186
- FIELDMAPS Team Website: <https://fieldmaps.weebly.com/>

Publications:

- [The Magnetic Field in the Milky Way Filamentary Bone G47.](#)

Molecular gas in a galaxy generally follows the spiral arms. In the Milky Way, the densest of this molecular gas can form long, velocity-coherent filaments parallel and in close proximity to the Galactic plane. These dense filaments make up the 'skeleton' of molecular gas of the Milky Way — akin to the dark dust lanes seen in nearby spiral galaxies — and thus have been called 'bones.' For the early stages of star formation, these bones represent the largest star-forming structures in the Galaxy, and previous studies suggest that magnetic fields are critical to their formation. Our pilot survey of 2 bones shows that HAWC+ can detect polarization over large angular extents with modest integration time. To understand how gas collects in the magnetized spiral potential, we propose a legacy survey to probe the magnetic fields across the entire extent of 8 additional bones (for a total of 10). We will use these observations in combination with new magnetohydrodynamical simulations of galactic formation of bones to investigate (1) the role of magnetic fields in the formation of bones, (2) how the field varies between arm and inter-arm bones, and (3) whether fields bend into filaments to build gas flows to the largest gravitational potential well.

5.2.2 SALSA: SOFIA Heralds a New Era of Measuring the Magnetic Fields of Galaxies

- Principal Investigator: *Enrique Lopez-Rodriguez (Stanford/KIPAC)*
- Plan ID: 08_0012
- FIELDMAPS Team Website: <http://galmagfields.com/>

Publications:

- [SOFIA Far-infrared Imaging Polarimetry of M82 and NGC 253: Exploring the Supergalactic Wind](#)
- [SOFIA/HAWC+ Traces the Magnetic Fields in NGC 1068](#)
- [The magnetic field across the molecular warped disk of Centaurus A](#)
- [The Strength and Structure of the Magnetic Field in the Galactic Outflow of Messier 82](#)
- [Extragalactic Magnetism with SOFIA \(Legacy Program\). I. The Magnetic Field in the Multiphase Interstellar Medium of M51](#)
- [Extragalactic Magnetism with SOFIA \(Legacy Program\) - II: A Magnetically Driven Flow in the Starburst Ring of NGC 1097](#)
- [Extragalactic Magnetism with SOFIA \(SALSA Legacy Program\). III. First Data Release and On-the-fly Polarization Mapping Characterization](#)
- [Extragalactic Magnetism with SOFIA \(SALSA Legacy Program\). IV. Program Overview and First Results on the Polarization Fraction](#)
- [Extragalactic Magnetism with SOFIA \(SALSA Legacy Program\): The Magnetic Fields in the Multiphase Interstellar Medium of the Antennae Galaxies](#)

Our team has made important and unexpected discoveries about the role of the magnetic fields in nearby galaxies. We have found a) that galaxies typically host large-scale and coherent magnetic fields along the spiral arms, b) magnetic field strengths of $\sim\mu\text{G}$ with similar contributions from the random and ordered field components, and c) magnetic fields oriented along galactic outflows that

are likely responsible for magnetizing the IGM. To date, these results have mostly emerged from single wavelength regimes: radio synchrotron polarization tracing the large-scale field structure in the ionized gas, and optical studies to investigate the effect of scattering and/or extinction by the ISM. These studies access the field on vastly different spatial scales and within different ISM phases. However, the effect of magnetic fields in dense regions of the ISM, outflows, and the ISM of merging galaxies are still poorly described. SOFIA/HAWC+ is key to provide a complete picture using far-infrared (FIR) polarimetric observations. This Joint Legacy Program aims to construct a comprehensive empirical picture of the magnetic field strength and structure in multiphase ISM of galaxies. Using HAWC+, we will conduct a FIR polarimetric survey covering the full disk of nearby galaxies.

Note: The SALSA legacy program is willing to share their custom-reduced data products with anyone interested in working with this dataset. Currently the legacy team is looking for a place to host their custom-reduced data but there is a high probability that they will eventually reside at IRSA under enhanced data products. Please refer to the SALSA legacy [data product documentation](#) for more info.

5.2.3 A Two-Color Polarimetric Survey of the Galactic Center

- Principal Investigator: *David Chuss (Villanova University)*
- Plan ID: 09_0054

Publications:

- [SOFIA/HAWC+ far infrared polarimetric large area CMZ exploration \(fireplace\) survey I: General results from the pilot program](#)

We propose a Legacy program to utilize HAWC+ to map the central region of the Galaxy at both 214 μm and 89 μm . We will utilize the shared-risk scan mode polarimetry observing strategy. The 214 μm map is proposed as a test case because the total integration time is modest. Upon successful completion of the 214 maps, (and the approval of the Cycle 9 TAC), we will proceed with the 89 μm survey in the second year of the program. The resulting data products will yield a transformative data set for understanding the magnetic fields in both the cool dust ring in the central 200 pc and the warmer dust component and its relationship to the hot features of the Galactic center. Such a data set would elucidate the role of the magnetic field in Galactic center dynamics from the 200 pc scale down to scales below a parsec.

5.2.4 Study of Interstellar Magnetic Polarization: A Legacy Investigation of Filaments (SIMPLIFI)

- Principal Investigator: *Thushara Pillai (Boston University)*
- Plan ID: 09_0215

Our understanding of star formation has been revolutionized by the insight that star-forming cores and hubs are embedded in complex filamentary networks that penetrate molecular clouds. Filaments differ greatly in their mass-to-length ratio -- which indicates the likelihood of star-forming fragmentation -- and the levels of associated star formation. Still, the exact role of

filaments in star formation remains unclear. In particular, magnetic fields might play an important role, as indicated by well-ordered polarized dust emission that imply strong magnetic fields. Here we propose SIMPLIFI, a SOFIA HAWC+ Legacy program that will carry out the first large-scale study of the magnetic polarization of filaments. The sample covers a wide range of mass-to-length ratios and star formation activities, in order to probe representative conditions for star formation. SIMPLIFI includes local filaments which are starless or form low-mass stars. SOFIA will resolve the column density and magnetic structure of filament ridges and cores much more clearly than previous work with Planck. SIMPLIFI also targets distant filaments that form clusters and massive stars, to reveal differences between regions of high-mass and low-mass star formation. Our project brings together an international team of observers, instrumentalists, and theorists to exploit these data to the fullest. This enables us to go beyond the standard Davis–Chandrasekhar–Fermi analysis, e.g. by using sophisticated flux-freezing models and complex numerical MHD simulations. A further unique feature of SIMPLIFI is our access to comprehensive imaging of gas density distributions and dynamics from dust and line observations. This enables SIMPLIFI to constrain the relative role of self-gravity, turbulence, and magnetic fields in star formation. SIMPLIFI will clarify the role of magnetic fields in star-forming filaments and will provide a framework to “simplify” the diversity of filament properties.

6. REFERENCES

- Kovács, A. (2006), Ph. D Thesis website: <https://thesis.library.caltech.edu/2400/1/thesis.pdf>
- Harper, D.A., et al. (2018), JAI, 7(4), doi: [10.1142/S2251171718400081](https://doi.org/10.1142/S2251171718400081)
- Li, P.S., et al. (2022a), MNRAS, 510, 6085-6109, doi: [10.1093/mnras/stab3448](https://doi.org/10.1093/mnras/stab3448)
- Li, P.S., et al. (2022b), MNRAS, 514, 3024-3040, doi: [10.1093/mnras/stac1527](https://doi.org/10.1093/mnras/stac1527)
- Lopez-Rodriguez, E. (2021), Nature Ast., 5, 604-614, doi: [10.1038/s41550-021-01329-9](https://doi.org/10.1038/s41550-021-01329-9)
- Lopez-Rodriguez, E., et al. (2021), ApJ, 923, 15, doi: [10.3847/1538-4357/ac2e01](https://doi.org/10.3847/1538-4357/ac2e01)
- Lopez-Rodriguez, E., et al. (2022), ApJ, 936, 24, doi: [10.3847/1538-4357/ac83ac](https://doi.org/10.3847/1538-4357/ac83ac)
- Müller, T.G., et al. (2016), A&A, 588, 21, doi: [10.1051/0004-6361/201527371](https://doi.org/10.1051/0004-6361/201527371)
- Pence, W.D., et al. (2010), A&A, 524, 40, doi: [10.1051/0004-6361/201015362](https://doi.org/10.1051/0004-6361/201015362)

APPENDIX

A. Response/Transmission Curves

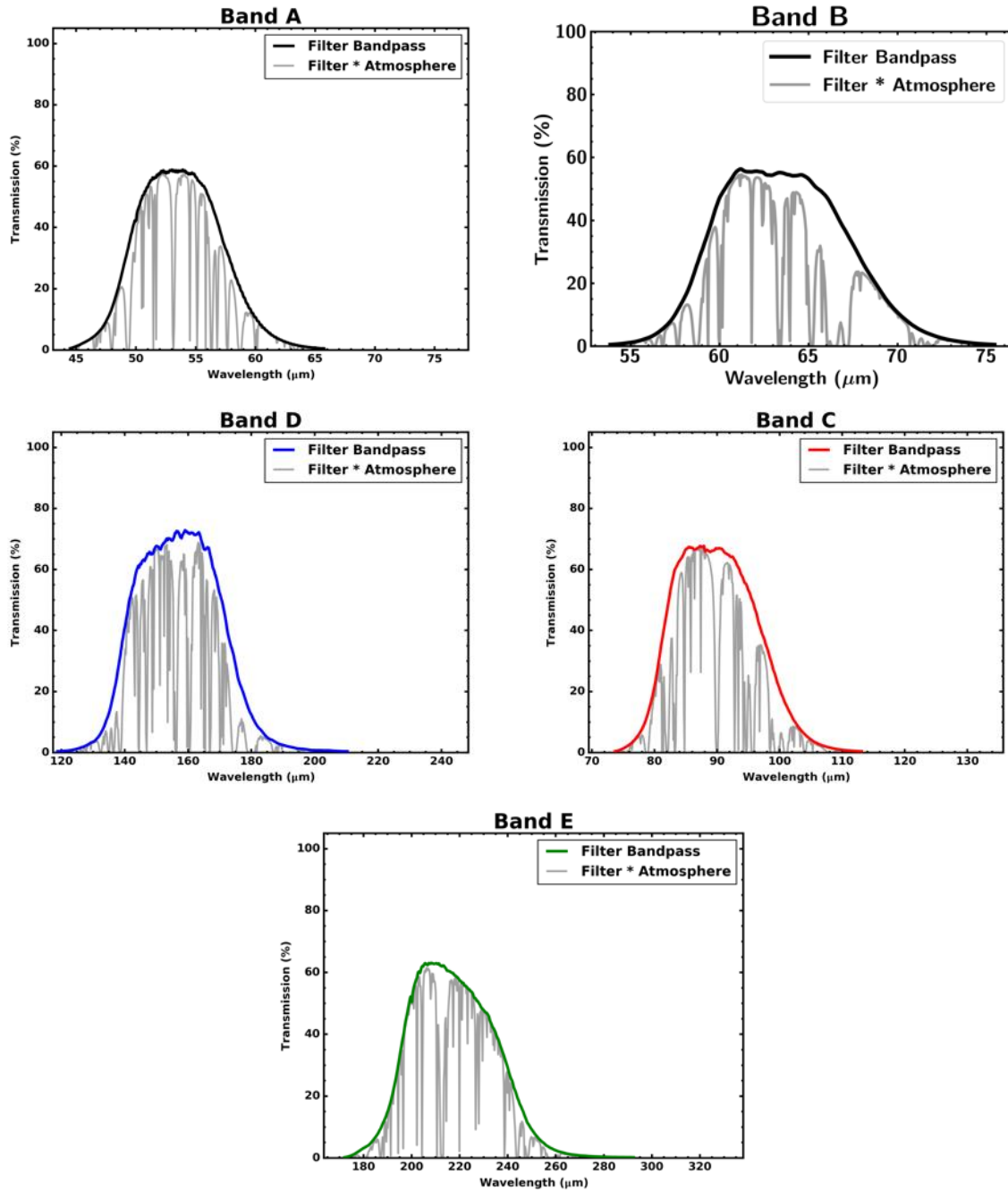


Figure 28 *Transmission Curves for HAWC+ Bands.*

B. Historical FWHM and Calibration Factors

Table 10: Measured Beam FWHM by Series (in arcsec)

Flight Series	Band A	Band B	Band C	Band D	Band E
OC4L	5.60		7.56	13.97	18.71
OC5E	5.21				20.14
OC5N	5.06		7.62	13.73	17.68
OC6I	5.74		8.25	14.53	19.35
OC6K	5.36		8.11	14.06	18.91
OC6T	5.35		8.10	13.76	18.34
OC7E	4.84	8.80	7.59	13.29	17.81
OC7F	5.36	8.66	7.67	13.31	17.81
OC7J	5.18	8.78	7.67	13.33	17.89
OC8E	5.56	8.19	7.8	13.24	18.74
OC8K	4.86	7.88	7.52	13.13	17.48
OC9D	5.26		7.70	13.35	17.82
OC9E	5.14		7.72	14.16	17.8
OC9H	5.16		7.73	13.36	17.86
OC9Q	4.93	7.14	7.52	13.03	17.70
OC9R	4.80	7.18	7.46	13.16	17.74
OC9W	4.78		7.46	13.05	17.68

Note - Measured beam FWHM by series (in arcsec) as geometric mean of FWHM_x and FWHM_y in planet calibration total intensity OTF maps.

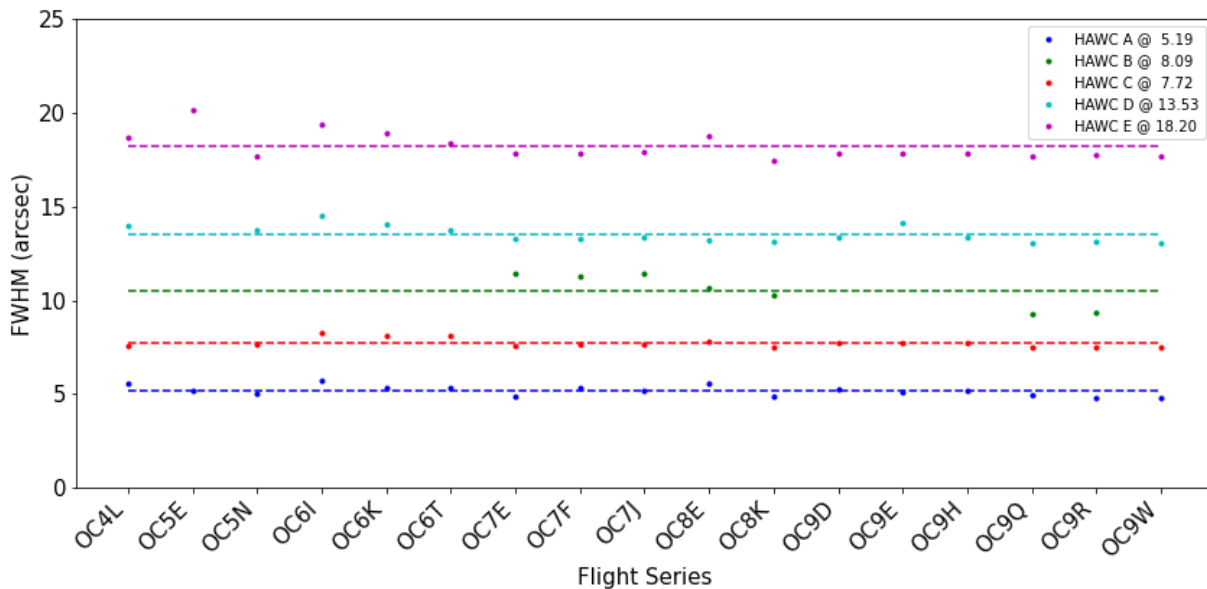


Figure 29 Measured FWHM for HAWC+ bands per flight series. HAWC+ Band B data has been scaled by 1.3 in the figure for display purpose.

Table 11: Calibration Factor for Total Intensity Observations by Series

Flight Series	Band A		Band B		Band C		Band D		Band E	
	CalFact	Error	CalFact	Error	CalFact	Error	CalFact	Error	CalFact	Error
OC4L	531.5866	47.6003			892.6512	89.9788	719.8665	72.1119	465.2139	65.857
OC5E	613.2932	19.0046			826.414	28.1817	669.9188	24.2275	461.9426	18.9066
OC5N	634.1024	90.29572			899.0834	83.35042	692.8599	76.38679	485.5034	43.85338
OC6I	618.0737	26.52911			860.9824	28.48989	644.6821	128.3532	450.6914	81.78254
OC6K	578.4474	115.5323			757.6982	87.38336	691.4336	51.44219	480.5152	27.14225
OC6T	830.6628	10.61458			1036.716	16.50611	877.8913	30.32823	539.7891	6.96667
OC7E	619.008	55.99365	343.1956	39.71574	811.9731	81.74573	721.2826	83.45177	487.2026	56.27482
OC7F	620.073	39.36235	312.4996	20.94531	773.4957	46.87186	634.0448	42.49148	467.5507	28.24875
OC7J	547.9513	55.3603	329.1015	46.56454	953.1502	134.9533	761.6469	107.8834	529.2494	74.85494
OC8E	622.3489	88.01688	281.6077	40.21946	800.8533	113.9648	682.2102	96.48536	500.6764	57.96494
OC8K	717.5589	101.4894	128.1026	14.88703	1008.653	90.52758	705.9126	70.61619	468.8898	54.41716
OC9D	573.6752	66.65963			815.7689	81.59452	627.4951	62.96433	492.4138	56.88125
OC9E	535.9423	53.61135			832.5478	166.51	609.9407	121.9889	601.886	120.3785
OC9H	639.0802	127.8161			841.6438	168.3288	703.8367	140.7674	503.8097	100.7637
OC9Q	484.1013	68.70025	170.6824	34.13908	542.2656	77.06308	381.0703	53.89993	287.4106	40.78539
OC9R	563.449	79.91132	164.3324	32.86796	673.8384	95.59992	491.3331	56.85928	287.895	33.35579
OC9W	631.725	73.35955			780.1998	90.14723	619.6513	71.84827	445.1431	44.76555
Average	605.919	68.61652			846.7939	92.28771	677.4844	82.21562	488.6206	59.4351

Table 12: Calibration Factor and Errors For Polarization Observations by Series

Flight Series	Band A		Band B		Band C		Band D		Band E	
	CalFact	Error	CalFact	Error	CalFact	Error	CalFact	Error	CalFact	Error
OC4L	529.3957	40.0502			814.1646	72.9318	681.2381	61.001	404.1233	80.8278
OC5E	594.4048	48.5514			814.1646	72.9318	627.8488	56.1653	526.6181	53.0031
OC5N					870.9155	9.87736			446.8184	89.36379
OC6I	647.1005	129.4201			761.0637	152.213	583.4052	116.6831	394.7503	22.20083
OC6K					738.5289	147.7058				
OC6T	631.6367	126.3274			1007.624	201.5248				
OC7E										
OC7F										
OC7J										
OC8E	531.7518	75.7286	295.8104	59.16499	784.1264	111.0828	562.6639	79.58747	487.0727	58.66605
OC8K										
OC9D	496.5045	49.658			755.8443	75.62645	634.6174	63.62476	453.3911	52.35888
OC9E	488.0999	69.03426			799.7852	159.9611	630.5219	72.97638	613.6634	122.742
OC9H	526.1056	60.81094			817.8876	116.5578	626.7139	56.1875	477.8131	42.76166
OC9Q	392.8583	78.57586			542.6094	108.5389	378.1522	53.51606	333.4682	47.39652
OC9R					695.426	139.0961	452.2578	52.28364	307.7514	43.72281
OC9W	523.415	74.0722			686.1202	79.24375	584.7185	67.5632	474.8973	67.69228
Average	542.0972	68.41572	295.8104	59.16499	784.2601	99.81317	616.466	71.72359	475.4609	65.51294

Calibration factors for total intensity observations by series, with errors, based on planet scans in OTFMAP observing mode are listed in [Table 11](#). Series in red are considered outliers and omitted from the overall average.

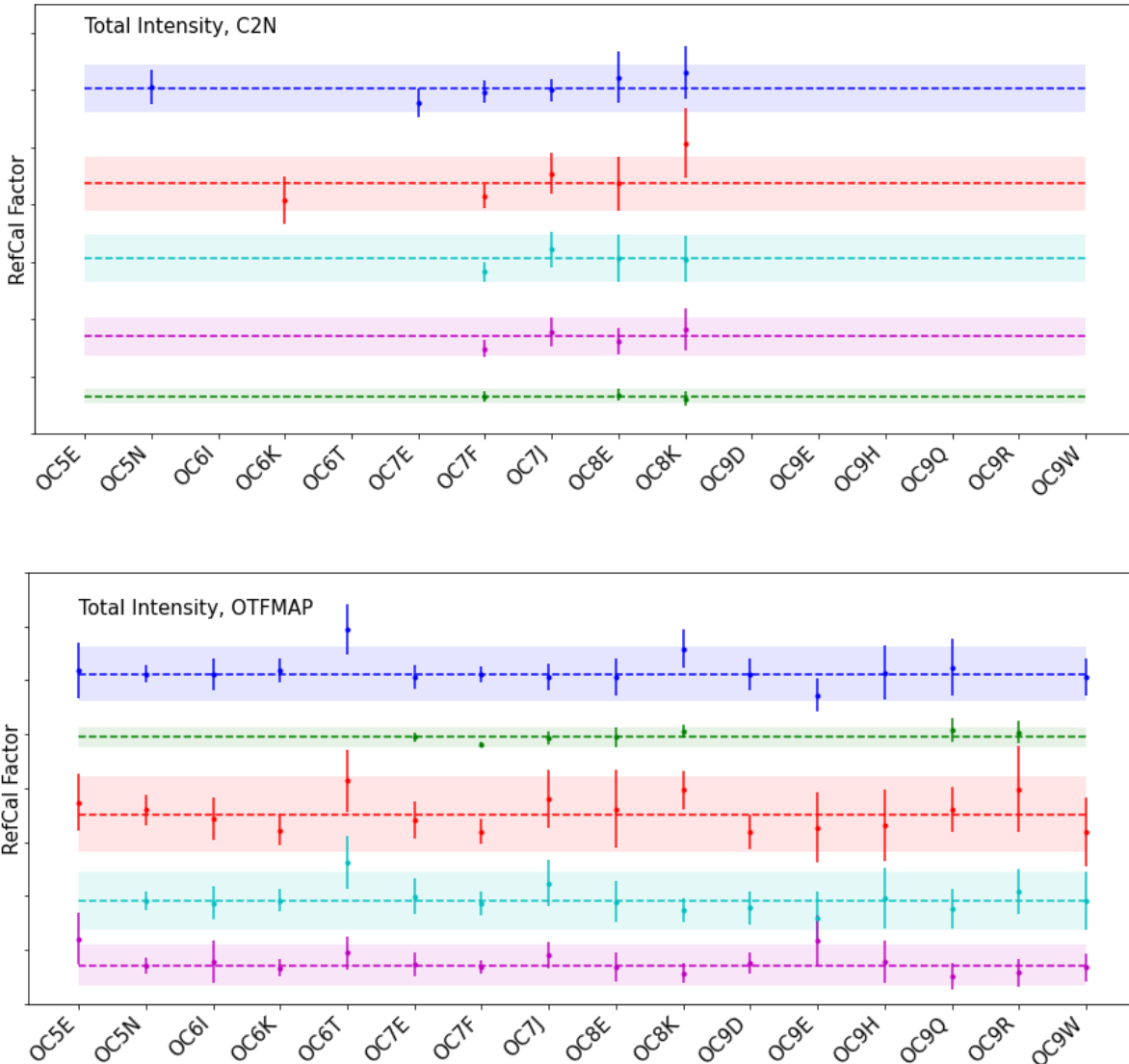


Figure 30 Trends in reference calibration factor, per band, derived from the total intensity observations in OTFMAP mode for each HAWC+ series. In this figure, data for HAWC+ Band A is shown in blue, Band B is green, Bands C is red, Band D is cyan, and Band E is magenta. The dashed line is the average reference calibration value for each of the bands. The colored shaded region shows the nominal $\pm 20\%$ calibration requirement.

The calculated calibration factors for polarization observations by series, with errors, based on planet scans in OTFMAP observing mode are listed in [Table 12](#) below and shown in the associated

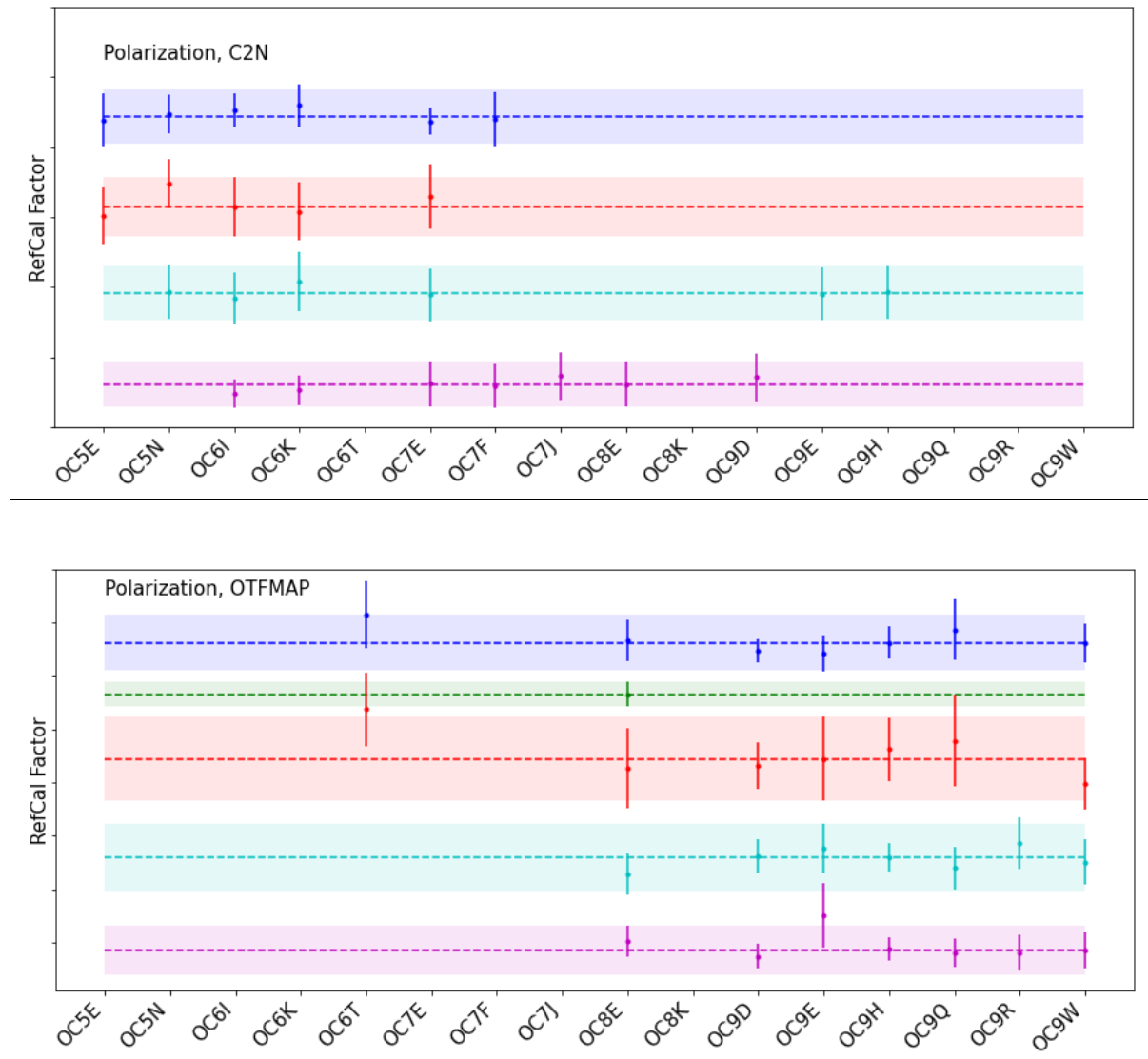


Figure 31. Series in red are considered outliers and omitted from the overall average.

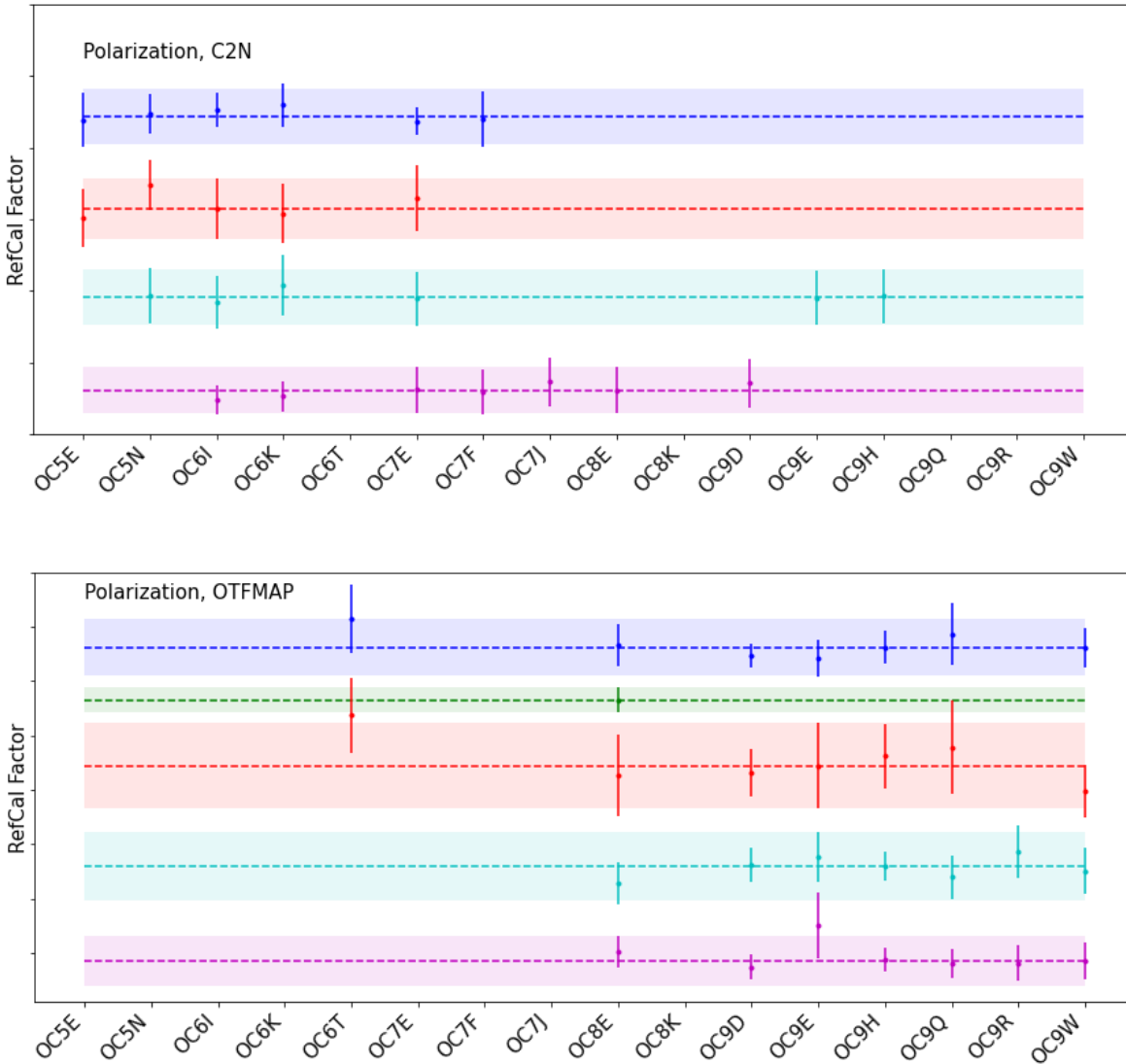


Figure 31 Trends in reference calibration factor, per band, for polarization observations for each HAWC+ series. In this figure, data for HAWC+ Band A is shown in blue, Band B is green, Band C is red, Band D is cyan, and Band E is magenta. The dashed line is the average reference calibration value for each of the bands. The colored shaded region shows the nominal $\pm 20\%$ calibration requirement.

C. Color Correction Factors

Table 13: Color Corrections K for HAWC+ Filters*

	53um	63um	89um	155um	216um
$\alpha=-4$	1.004	1.003	1.004	1.005	1.005
$\alpha=-3$	1.000	1.000	1.000	1.000	1.000
$\alpha=-2$	1.000	1.000	1.000	1.000	1.000
$\alpha=-1$	1.004	1.003	1.004	1.005	1.005

$\alpha=0$	1.011	1.008	1.011	1.016	1.015
$\alpha=1$	1.021	1.016	1.023	1.031	1.031
$\alpha=2$	1.035	1.027	1.038	1.053	1.052
$\alpha=3$	1.053	1.041	1.057	1.080	1.079
T=10000K	1.035	1.027	1.038	1.053	1.052
T=5000K	1.035	1.027	1.037	1.052	1.052
T=3000K	1.035	1.027	1.037	1.052	1.052
T=1000K	1.033	1.026	1.036	1.051	1.051
T=750K	1.032	1.025	1.036	1.051	1.051
T=500K	1.030	1.024	1.034	1.050	1.050
T=300K	1.026	1.022	1.032	1.048	1.049
T=200K	1.022	1.019	1.029	1.046	1.047
T=150K	1.017	1.015	1.026	1.044	1.046
T=100K	1.007	1.009	1.020	1.039	1.042
T=70K	0.998	1.002	1.012	1.033	1.038
T=50K	0.990	0.995	1.003	1.024	1.032
T=30K	1.004	0.995	0.990	1.006	1.018

* The factor K converts an input flux density to that of a nominal 'flat spectrum' source at the mean wavelength of the filter. The input spectral shape is described by a power law ($F_n \mu n^a$) or a blackbody with a temperature T .

Table 14: Isophotal Wavelengths for HAWC+ Filters

$\alpha=-4$	53.656	63.342	89.478	156.897	217.528
$\alpha=-3$	53.560	63.253	89.305	156.480	216.969
$\alpha=-2$	53.467	63.166	89.137	156.073	216.416
$\alpha=-1$	53.373	63.079	88.969	155.665	215.864
$\alpha=0$	53.280	62.995	88.805	155.266	215.318
$\alpha=1$	53.189	62.912	88.643	154.872	214.777
$\alpha=2$	53.098	62.830	88.484	154.483	214.241
$\alpha=3$	53.008	62.750	88.326	154.097	213.713
T=10000K	53.099	62.831	88.485	154.485	214.244
T=5000K	53.100	62.832	88.487	154.487	214.246
T=3000K	53.103	62.834	88.489	154.490	214.249
T=1000K	53.114	62.842	88.500	154.506	214.264
T=750K	53.120	62.846	88.506	154.513	214.272
T=500K	53.132	62.856	88.518	154.530	214.287
T=300K	53.160	62.875	88.544	154.563	214.320
T=200K	53.200	62.904	88.580	154.608	214.362
T=150K	53.248	62.937	88.619	154.655	214.406
T=100K	53.372	63.019	88.711	154.759	214.501
T=70K	53.676	63.179	88.861	154.912	214.635
T=50K	-	64.014	89.154	155.153	214.839
T=30K	-	-	-	155.972	215.441

Table 15: Wavelengths for HAWC+ Filters

	53um	63um	89um	155um	216um
Mean λ	53.560	63.253	89.305	156.480	216.969
Pivot λ	53.280	62.995	88.805	155.266	215.318
Prime λ	53.373	63.079	88.969	155.665	215.864

D. Important HAWC+ Header Keywords

Some of the more important header entries for HAWC+ are explained below. The common values the header keywords have for science data are also provided. Other values may be possible, but only in engineering data. Review of other general keywords in header that are not specific to HAWC+ or not covered below are in the *SOFIA FIT Keyword Dictionary* available at the [IRSA SOFIA Data Processing website](#).

The header information below is divided into major subsections of the HAWC+ header, which are demarcated in the headers with the same names as the table titles. HAWC+ did commissioning and science observations from Cycle 4 to Cycle 9, and as the observatory software changed over time, housekeeping data and FITS keywords were added or modified. Old keywords were kept for backwards compatibility, but over time became antiquated. Keywords below that may not be reliable or have been changed over time are marked with an asterisk and a comment containing further information.

--- DCS DATA COLLECTION ---		
FITS Keyword	Value	Description
CHOPPING	T/F	T if telescope was chopping during observation (should never be F)
NODDING	T/F	T if telescope was nodding during observation (this will rarely be F)
DITHER	T/F	T if telescope was dithering during observation
MAPPING	T/F	Should always be F (HAWC+ does not utilize the telescope's default mapping functionality)
SCANNING	T/F	T is the telescope was scanning.
NONSIDE	T/F	This will be set to T if the target being observed is a non-sidereal target
MISSN-ID	[STRING]	Unique mission identifier, identifying the SOFIA flight.
AOR_ID	[STRING]	Unique astronomical observation request identifier

OBS_ID	[STRING]	Unique SOFIA identifier made up of MISSN-ID, AOR_ID and the file number
--- DCS INSTRUMENT ---		
FITS Keyword	Value	Description
INSTCFG	TOTAL_INTENSITY POLARIZATION	HAWC+ instrument configuration either total_intensity (imaging) or polarization.
INSTMODE	C2N (NMC) OTFMAP	Mode of data collection: symmetric nod matched chop mode OR on-the-fly (OTF) mapping mode.
EXPTIME	[FLOAT]	Nominal on-source integration time. This is the time that should be used for science.
SPECTEL1	HAW_A HAW_B HAW_C HAW_D HAW_E	Filter used during observations
SPECTEL2	HAW_HWP_A HAW_HWP_B HAW_HWP_C HAW_HWP_D HAW_HWP_E HAW_HWP_Open	Halfwave plate used for polarimetric observations. For total intensity observations HAW_HWP_Open is used.
WAVECENT	[FLOAT]	Calculated mean wavelength of the filter based upon instrument throughput
--- DCS ARRAY DETECTOR ---		
FITS Keyword	Value	Description
DETECTOR	HAWC	Detector name.
PIXSCAL	[FLOAT]	The pixel scale for HAWC+ filters. The pixel scale is different for different HAWC+ filters. For exact values see Table 1.
--- DCS CHOPPING ---		
FITS Keyword	Value	Description

CHPFREQ	[FLOAT]	Full cycle chop rate in Hz
CHPSYM	2_point_symmetric no_chop	Chop symmetry. no_chop is used for OFTMAPs
CHPAMP1	[FLOAT]	Chop amplitude in arcsec
CHPCRSYS	ERF SIRF	This the coordinate systems the chopping is being defined in: ERF is the Equatorial Reference Frame (aka Sky coordinates) and SIRF is the Science Instrument Reference Frame (aka Array coordinates)
CHPANGLE	[FLOAT]	Actual chop angle in degrees in the CHPCRSYS coordinate system measured by telescope encoders
--- DCS NODDING ---		
FITS Keyword	Value	Description
NODTIME	[FLOAT]	Integration time at each nod position.
NODN	[INTEGER]	Number of nods requested
NODAMP	[FLOAT]	Total distance telescope nodded in arcsec (aka “nod throw” since it is not really an amplitude)
NODPATT	ABBA	HAWC+ has only one nod pattern, ABBA.
*NODSTYLE	NMC	HAWC+ has only one nod style, NMC.
NODCRSYS	ERF SIRF	This is the coordinate system the noddng is being defined in: ERF is the Equatorial Reference Frame (aka Sky coordinates) and SIRF is the Science Instrument Reference Frame (aka Array coordinates)
NODANGLE	[FLOAT]	Actual nod angle in degrees in the NODCRSYS coordinate system measured by telescope encoders
--- DCS DITHERING ---		
FITS Keyword	Value	Description

DTHCRSYS	ERF SIRF	This is the coordinate system the dithering is being defined in: ERF is the Equatorial Reference Frame (aka Sky coordinates) and SIRF is the Science Instrument Reference Frame (aka Array coordinates)
DTHXOFF	[FLOAT]	Dither offset in x coordinates and in DTHUNITS defined in DTHCRSYS coordinate system
DTHYOFF	[FLOAT]	Dither offset in y coordinates and in DTHUNITS defined in DTHCRSYS coordinate system
DTHNPOS	[INTEGER]	Number of dither positions
DTHUNITS	STRING	Dither units; pixels or arcsec
DTHSCALE	[FLOAT]	Dither scale in DTHUNITS defined in DTHCRSYS coordinate system
--- DCS SCANNING ---		
FITS Keyword	Value	Description
SCNPATT	STRING	Scan pattern: Lissajous or Raster
SCNRATE	[FLOAT]	Scan rate in arcsec per second
SCNANGLS	[FLOAT]	Starting scan angle in degrees
SCNANGLF	[FLOAT]	Final scan angle in degrees
SCNAMPEL	[FLOAT]	Scan amplitude in elevation in arcsec
SCNAMPXL	[FLOAT]	Scan amplitude in cross elevation in arcsec
SCNDUR	[FLOAT]	Total scan duration
SCNSTEPS	[INTEGER]	Number of raster scan steps
SCNLEN	[FLOAT]	Size of raster scan in arcsec
SCNSTEP	[FLOAT]	Raster scan step size in arcsec
--- PIPELINE RELATED KEYWORDS (IMAGING) ---		
FITS Keyword	Value	Description

ASSC_AOR	STRING	If data is processed in a multi-mission procedure then this is the list of all the associated AORs
ASSC_MSN	STRING	If data is processed in a multi-mission procedure then this is the list of all the associated mission IDs
CALFCTR	[FLOAT]	Calibration factor (Me/s/Jy), same as the “reference calibration factor” given in the HISTORY section of the header (see Section 4.3.1). Used as a divider for OPS or MRG files to convert to CAL or STD files
ERRCALF	[FLOAT]	Calibration factor uncertainty (Me/s/Jy)
LAMREF	[FLOAT]	Reference wavelength (microns), as given in Table 7.2-2.
LAMPIVOT	[FLOAT]	Pivot wavelength (microns), as given in Table 7.2-2.
REFCALF3	[STRING]	Filename of the calibration file found in the pipeline
COLRCORR	[FLOAT]	Color correction factor
DATAQUAL	[STRING]	Data quality keyword either NOMINAL or USABLE

D.1 HISTORY Section of HAWC+ FITS Data Headers

Below is an example of selected parts of the HISTORY section at the bottom of the HAWC+ FITS headers containing information that may be of importance or require further explanation. This section of the FITS headers is annotated with explanations.

<p>HISTORY Merged Files: HISTORY OBS_ID: P_2019-07-18_HA_F598-07_0081_2-018 HISTORY OBS_ID: P_2019-07-18_HA_F598-07_0081_2-019 HISTORY OBS_ID: P_2019-07-18_HA_F598-07_0081_2-020 HISTORY OBS_ID: P_2019-07-18_HA_F598-07_0081_2-023 HISTORY OBS_ID: P_2019-07-18_HA_F598-07_0081_2-025 HISTORY OBS_ID: P_2019-07-18_HA_F598-07_0081_2-026</p> <p>HISTORY Reduced: fluxjump 2023-08-09_15:49:59 HISTORY CONFIG: config/pipeconf.cfg HISTORY CONFIG: config/date_overrides/pipeconf_oc7e.cfg</p>	<p>< This section includes the file identifiers used in this reduction. This is basically a list of input files.</p> <p>< This section has detailed on any specific flags used during data processing. In this example we see that the fixjumps flag was used.</p>
---	--

HISTORY Reduced: demodulate 2023-08-09_15:50:41
HISTORY demodulate: chop_tol=0.2
HISTORY demodulate: nod_tol=5.0
HISTORY demodulate: hwp_tol=2.0
HISTORY demodulate: az_tol=5000000.0
HISTORY demodulate: el_tol=5000000.0
HISTORY demodulate: track_tol=beam
HISTORY demodulate: track_extra=[0.0, 0.0]
HISTORY demodulate: chopphase=True
HISTORY demodulate: checkhwp=True
HISTORY demodulate: phaseoffset=0.0

HISTORY Using reference files:
HISTORY hawc_plus/response/rfit_am_20181128.txt
HISTORY hawc_plus/response/rfit_alt_20181128.txt
HISTORY Reference ZA=45.0, altitude=41.0
HISTORY Telluric correction factor for ZA=38.95, altitude=38.0255:
HISTORY 1.1333511855581766

HISTORY Flux calibration information:
HISTORY Using reference file: hawc_plus/ref_calfctr/OC7E_20230815.txt
HISTORY Average reference calibration factor:
HISTORY 45.74922 +/- 9.14985
HISTORY Data has been divided by cal factor to convert
HISTORY from counts to Jy

< Each pipeline module will have its own section with the list of parameters used to reduce the data.

< Section identifying the reference files and parameters used during opacity correction.

< Section identifying the flux calibration reference files and parameters used to flux calibrate the data.